DME/TACAN Multipath Impact on GNSS L5/E5a Airborne Receivers Part I: C/N0 Degradation Model

NICOLAS GAULT
AXEL GARCIA-PENA
ALEXANDRE CHABORY
CHRISTOPHE MACABIAU
LOÏC SHI-GARRIER
École Nationale de l'Aviation Civile, Toulouse, France

This article is the first part of a two-part manuscript addressing the DME/TACAN multipath (MP) impact on the future airborne GNSS Dual-Frequency Multi-Constellation (DFMC) GNSS L5/E5a receiver correlator input. GNSS L5/E5a signals and DME/TACAN pulsed signals share the same Aeronautical Radionavigation Service (ARNS) frequency band with consequent interference between the two systems. The current GNSS signal C/N_0 degradation model for future airborne GNSS DFMC receivers due to DME/TACAN pulsed signals is expressed at the DMFC correlator input and is standardized in different civil aviation documents. This model considers the introduction of a temporal blanker at the DMFC Radio-Frequency Front-End (RFFE) block output to mitigate the DME/TACAN pulsed signals and thus, relies on the definition of the above blanker pulse width (pw^{eq}) and the below blanker equivalent pulse width (PW^{eq}). However, this model did not consider the presence of DME/TACAN pulsed signals MP.

Indeed, the DME/TACAN MP impact on the GNSS signal C/N_0 degradation was never inspected while it could be significant, especially at low altitude. The objective of this paper is thus to update the C/N_0 degradation model by considering DME/TACAN MP impact generated by ground scatterers. This is done by updating pw^{eq} and PW^{eq} formulas which require the knowledge of the MP delays and Peak Envelope Powers. In particular, this paper proposes two models of the DME/TACAN MP impact, the statistical and the fixed environment models, where the main difference is the modelling of the additional phase generated by the channel environmental condition θ_e; as an uniform variable in the statistical model and as a constant in the fixed environment model. As a consequence, the Pulse Independency Condition (PIC) is satisfied (power of the sum of received DME/TACAN pulses is equal to the sum of the received pulses power) for the statistical model, which is not always true for the fixed environment model. The two models are proposed to cover different needs. The statistical model is a low complexity model completely defined by closed-form formulas, and is proposed to be used for standardization purposes. The fixed environment model is a higher complexity model with two main purposes. First, the fixed environment model is able to provide the C/N_0 degradation for one specific set of DME/TACAN signal conditions. Second, the fixed environment model is used to inspect the limitations of the statistical model by identifying geographical zones where the received power of the DME/TACAN MP signals generated by the ground scatterers only loosely fulfills the PIC.

I. INTRODUCTION

The nominal processing of Global Navigation Satellite System (GNSS) received signals can be affected by noise as well as received additive signals such as multipath (MP) and Radio Frequency Interference (RFI) [1]. GNSS L5/E5a interference environment is predominantly dominated by pulsed interferences such as DME/TACAN and JTIDS/MIDS [1], [2]. In the context of civil aviation, the RFI impact on a GNSS receiver is standardized in the United States by the Radio Technical Commission for Aeronautics (RTCA), in Europe by the European Organization for Civil Aviation Equipment (EUROCAE) and internationally by the International Civil Aviation Organization (ICAO).

In the standards of these standardization bodies, the RFI impact is usually modelled as the GNSS signal C/N_0 degradation induced by the RFI signals at the airborne GNSS receiver correlator input, which is determined as the difference between the nominal C/N_0 (where only the useful GNSS signal is present) and the effective C/N_0, $C/N_{0,\text{eff}}$ (where the GNSS and the RFI signals are present) [1]. The effective noise Power Spectrum Density (PSD), $N_{0,\text{eff}}$, is defined as the increased noise PSD due to the RFI signals presence with respect to the nominal noise PSD, N_0 at the GNSS correlator input. The first mathematical models of $N_{0,\text{eff}}$ were provided for non-white PSD, for continuous waveform (CW) RFI as well as for pulsed CW RFI in [3],[4] and [5], respectively.

However, an additional effort was required to further adapt the $N_{0,\text{eff}}$ for the future airborne GNSS Dual-Frequency Multi-Constellation (DFMC) receivers, where a temporal blanker is assumed to be implemented in the Radio-Frequency Front-End (RFFE) block of the GNSS DFMC receiver by the civil aviation standards to mitigate the impact of the pulsed RFI observed in the L5/E5a band [1]. The role of the temporal blanker is to set to zero the received signal samples having its instantaneous power envelope higher than a certain threshold (interference detection) [6]. In the process, the useful GNSS signal is also blanked, and thus, considering the loss of power on the useful GNSS signal, on the RFI signals and on the noise induced by the blanker, a statistical model of $N_{0,\text{eff}}$ was proposed in the RTCA DO-292 standard [1], resulting from the efforts of [7],[8] and [9].

In this model, $N_{0,\text{eff}}$ is defined as a function of the percentage of samples set to zero by the blanker, denoted as blanker duty cycle, (bdc), and the below-blanker interfering-signal-to-thermal-noise ratio, R_{I}, customized for DME/TACAN [1],[10] and JTIDS/MIDS [1],[11] RFI signals. The values of bdc and R_{I} depend on the RFI scenario (number

of emitting beacons, interference received power at the aircraft antenna port, etc.) and a worst-case scenario was found at Harrisburg P.A, at high altitude (FL400), where the C/N_0 degradation was determined equal to 7.34 dB, after correcting the identified numerical error in [1].

Over the last years, in the RTCA DO-292 [1] updating process, the temporal blanker implementation, which mechanism was not clearly defined in [1], was addressed in [12] and a more accurate R_I mathematical model, based on the exact derivation of the Spectral Separation Coefficient (SSC), which is defined as the integral of the multiplication between the local replica PSD and RFI signal PSD, was proposed in [13]. Moreover, this more accurate model was later used in [10] to refine the GNSS signal C/N_0 degradation induced by the DME/TACAN RFI signals only at the airborne GNSS receiver correlator input.

However, there is still remaining work to make the C/N_0 degradation model as accurate and realistic as possible. Indeed, two recent experimental studies from 2019 and 2021 have shown I/Q samples recordings exhibiting high blanking levels not predicted by the bdc mathematical model developed in [1]; the reason for this increase was the presence of strong DME/TACAN multipath (MP) [14],[15]. The I/Q samples recordings were obtained by WAAS reference stations in the vicinity of Honolulu (Hawaii) and Palmdale (California) airports. The relevance of these two experiments is very important considering the stronger focus given to low altitude scenarios in the updated standards. Indeed, the DME/TACAN beacons/aircraft RFI scene considered in the standards is such that the DME/TACAN beacons situated on the ground transmit a signal near the L5 frequency (1176.45 MHz) to the aircraft situated at an altitude range from a few hundred of meters to several kilometers and a slant range from the beacons of a few tens of kilometers. In this scene, many elements (buildings, electric pylons, trees, etc.) situated in the Radio Line Of Sight (RLOS) of the emitting DME/TACAN beacons are generating MP and must be considered, even if the scattered power may be very small. The elements generating DME/TACAN MP are called scatterers and DME/TACAN pulses received from MP are referred to echoed pulses or echoes in this work. For a more complete characterization of the DME/TCAN beacons/aircraft propagation channel, the reader is referred to Part II of this work [16]. DME/TACAN pulses received from MP are referred to echoed pulses or echoes in this work.

Therefore, the findings of the experimental studies combined with the considered RFI scene show that there is a need for characterizing the DME/TACAN MP impact since echoed pulses affect the receiver in the same manner as the direct pulse: echoes could trigger the blanking threshold and thus increase bdc or simply increase R_I [15]. This characterization is all the more important as the GNSS L5/E5a RFI link budget margin is expected to be very small [13] and thus, all the physical effects impacting the C/N_0 degradation must be modelled as realistically as possible to guarantee that the link margin is still positive. Moreover, to the authors' best knowledge, no GNSS signal C/N_0 degradation mathematical model considering DME/TACAN MP effect in the $N_{0,\mathrm{eff}}$ derivation has either been proposed in the literature or in the standard, where a simple propagation channel model only considering Line-of-Sight free-space loss was used [1].

For these reasons, the general objective of this two-part manuscript is to conduct a DME/TACAN MP impact analysis on the GNSS signal C/N_0 degradation computation at the GNSS DFMC correlator input. More specifically, this manuscript (part I) updates the R_I and bdc analytical models proposed in [1] to accurately consider echoes in the C/N_0 degradation computation. For a complete characterization of the DME/TACAN beacons/aircraft propagation channel model necessary to compute the final C/N_0 degradation, the reader is referred to Part II of this work [16].

In particular, two models are proposed in this manuscript to update R_I and bdc: the statistical and the fixed environment models. On one hand, the statistical model assumes that the additional received DME/TACAN signal phase offset generated by any physical effect such as the modification of the atmospheric refraction or the modification of the Dyadic Fresnel reflection and transmission coefficients of the scatterers (due to the DME/TACAN beacon/aircraft environment time dependent properties) [17], follows an uniform distribution on $[0,2\pi)$. The DME/TACAN beacon/aircraft environment time dependent properties are defined in this article as the atmosphere temperature, pressure or humidity, the weather or the time dependent scatterers properties (open windows, closed shutters, constructions, etc.). This model allows to find a statistical average of the C/N_0 degradation for a single aircraft position in a given aircraft trajectory assuming that the DME/TACAN beacon/aircraft environment time dependent properties at a specific given time are unknown. The strength of the statistical model is that it is a simple and low complex model to apply once the propagation channel model parameters have been obtained. Its weakness is that it may not be suitable to represent all phase offsets realizations since only a statistical average of the C/N_0 degradation is provided.

On the other hand, the fixed environment model assumes that the phase offset produced by the physical effects of the DME/TACAN beacon/aircraft environment time dependent properties can be assumed to be constant over a short time T_0 and thus that additional received DME/TACAN signal phase offset generated by the environment is also constant during that time. Therefore, this model allows to find a statistical average (conditioned on the known phase offset) of the C/N_0 degradation for a small segment of an aircraft trajectory which does not last longer than T_0. The strength of the fixed environment model is that it is in theory able to provide the C/N_0 degradation for any phase offset realizations. However, its complexity may be too high to be applied in some RFI environments where the number of scatterers is large.

The statistical model presented in this work is later used in Part II of this two-parts manuscript to determine the additional C/N_0 degradation due to DME/TACAN only generated by echoed pulses at two low-altitude operational hot-spots:

JALTO (USA) FAF and TIXAK (Europe) FAF, which are two single points of the approach of the Philadelphia and Frankfurt airports [16]. Note that the proposed statistical model was initially presented in [18] by the same authors but was never mathematically derived. Also note that, for concision purposes, the term C/N_0 degradation is used in this paper to designate the C/N_0 degradation to the useful GNSS signal in presence of DME/TACAN RFI signals at the GNSS DFMC correlator input of the airborne DMFC receiver. Likewise, the terms referring to MP (scatterers, echoed pulses, echoes) are always associated with DME/TACAN MP, since GNSS MP study is out of the scope of this paper.

The article is organized as follows. Section II provides an overview of the DME/TACAN system and signal description and the current (MP-free) C/N_0 degradation model as described in [1]. Section III introduces the theoretical derivation of the statistical C/N_0 degradation model considering MP. Section IV presents the fixed environment C/N_0 degradation model theoretical analysis considering MP. Section V is dedicated to the validation of the statistical and fixed-environment models by means of DME/TACAN RFI signals simulation. Section VI concludes the analysis.

II. CURRENT STATISTICAL DME/TACAN C/N_0 DEGRADATION MODEL

This section introduces a detailed tutorial for the statistical, MP-free, GNSS C/N_0 degradation when considering DME/TACAN as the only RFI source. Section II.A is a state-of-the-art review of DME and TACAN systems and signal description. Section II.B introduces the GNSS DFMC receiver generic structure, reviews the general MP-free $N_{0,\text{eff}}$ model as provided in [1] and, in top of applying the model to the DME/TACAN RFI signals, presents a detailed list of the assumptions only provided at high-level in [1] in order to derive the R_I and bdc mathematical models.

A. DME/TACAN System and Signal Description

DME, and its military equivalent, TACAN, are two systems used by aircraft to determine their distance to a position-known ground beacon. The airborne interrogator sends interrogations to the beacons. Once the interrogation is detected, the beacon transponder replies to the interrogation. The slant range (distance between the two systems) is then determined by measuring the time elapsed between each pulse transmitted by the interrogator and the reception of its corresponding reply pulse from the transponder. This delay corresponds to twice the distance between the aircraft and the beacon, as well as a fixed processing time inside the ground station. DME and TACAN full systems operation are described in [19] and [20], respectively. The main difference between the two systems is the TACAN beacon rotating antenna allowing the aircraft to have an azimuth information in addition to the slant range. However, from an RFI signal analysis point of view, there is no difference in addition to the Pulse Repetition Frequency (PRF): 2700 and 3600 for DME and TACAN, respectively.

Among all the signals' transmissions between the DME/TACAN system's equipment, only the reply pulses emitted by ground beacon transponders operating in mode X are considered as a relevant RFI as they emit their signals between 962 and 1213 MHz, which overlaps the GNSS L5/E5a band, equal to [1166.45; 1186.45] MHz [1]. The other potential threats such as the DME/TACAN other operating modes (Y, W or Z) and DME/TACAN interrogations sent by nearby aircraft have been demonstrated to be insignificant: signals emissions in modes Y,W and Z are out of band (and thus attenuated by a 70dB rejection filter) and minimum allowable aircraft separation distances are sufficient to significantly reduce the impact of interrogations sent by nearby aircraft [1].

The beacon transponder replies are thus the RFI investigated in this work. Without MP, a single beacon emitted reply $s_{\text{bb}}(t)$ at baseband is a composite pulse composed of two Gaussian pulses such that

$$\begin{aligned} s_{\text{bb}}(t) &= g(t) + g(t-\Delta t) \\ g(t) &= e^{-\frac{\alpha}{2}t^2}, \end{aligned} \tag{1}$$

where $\alpha = 4.5 \cdot 10^{11}$ s^{-2} is a constant of pulse and Δt = 12 μs is the inter pulse time separation for mode X. Fig. 2 (green curve) provides an example of a baseband emitted pair. The signal s_{bb} is then modulated by a cosine before its broadcasting to the aircraft. Fig. 2 (blue curve) provides an example of a modulated emitted pair in presence of noise.

Multiple aircraft are simultaneously communicating with different beacons and therefore multiple replies may be received by a single aircraft. Therefore, the received signal $v(t)$ at an aircraft's receiving antenna port without considering multipath, during an observation period $[0, T_0]$, is mathematically modelled as

$$\begin{aligned} v(t) &= \sum_{m=1}^{M}\sum_{\kappa=1}^{\text{K}_m} A_m s_{\text{bb}}\left(t - t_m^\kappa - \tau_m(t)\right) \cdot \\ &\qquad \cos\left(2\pi\left(f_m + f_{D,m}\right)t + \theta_m^\kappa\right), \\ A_m &= \sqrt{2\text{PEP}_m}. \end{aligned} \tag{2}$$

The index m is used to identify the different broadcasting beacons, where M is the number of DME/TACAN emitting beacons in the aircraft Radio Line Of Sight (RLOS).

The index κ is used to identify the emitted pulse pair, where K_m is the number of pulse pairs sent by beacon m during $[0, T_0]$ and is assumed to be known. When the time of observation T_0 is long enough ($T_0 \to \infty$), K_m tends to $\text{PRF} \cdot T_0$.

The scalars A_m and PEP_m are respectively the amplitude and peak envelope power of the received composite pulses from beacon m assumed to be constant inside $[0, T_0]$.

The random variable t_m^κ is the emitted time of pair κ from beacon m and is modelled to follow an uniform distribution

over $[0, T_0]$ ($t_m^\kappa \sim U[0, T_0]$), as the emission of emitted pairs is assumed to follow a Poisson process [1] and K_m is assumed to be known.

The scalar $\tau_m(t)$ is the associated propagation time delay which evolves with time. For a short time T_D ($t \in [-T_D, T_D]$), $\tau_m(t)$ can be approximated by its first-order Taylor's expansion, $\tau_m(t)$ as

$$\tau_m(t) = \tau_m(0) + t \left. \frac{d\tau_m(t)}{dt} \right|_{t=0}. \quad (3)$$

The frequencies f_m and $f_{D,m}$ are the carrier and Doppler frequencies of beacon m signal, respectively. The expression of $f_{D,m}$ is given by, from (3),

$$f_{D,m} = -2\pi f_m \left. \frac{d\tau_m(t)}{dt} \right|_{t=0}. \quad (4)$$

The random variable θ_m^κ is the carrier phase offset of emitted pair κ of beacon m, modelled as

$$\theta_m^\kappa = \theta_{0,m}^\kappa + \theta_{\mathrm{D},m} + \theta_{\mathrm{e},m} \bmod 2\pi, \quad (5)$$

where the initial phase $\theta_{0,m}^\kappa$ is the phase generated at each pair k of beacon m generation. Assuming that the transponder is switched on and off each time a pulse pair is emitted, $\theta_{0,m}^\kappa$ can be modelled as an uniform variable on $[0,2\pi)$ and is independent for $m \neq m'$ and $\kappa \neq \kappa'$. The phase $\theta_{\mathrm{D},m}$ is the additional carrier phase due to the initial propagation time delay $\tau_m(0)$, i.e., from (3),

$$\theta_{\mathrm{D},m} = -2\pi f_m \tau_m(0). \quad (6)$$

Finally, the additional phase offset $\theta_{\mathrm{e},m}$ is the offset introduced by the physical effects generated by the propagation channel environment (weather, atmosphere temperature, pressure and humidity, etc.). Physical effects are assumed not to change inside interval $[0, T_0]$ between pulse pair emissions (and thus $\theta_{\mathrm{e},m}$ does not to depend on κ) given the relatively low time interval between pulse emission (as high as 1.4 ms as specified in [19]). Its mathematical modelling depends on the targeted application/analysis; two different assumptions are considered in this work; the statistic assumption in Section III.A and the fixed environment assumption in Section IV.A, respectively.

B. Current RTCA DO-292 Statistical C/N_0 Degradation Model

In this section, a generic airborne GNSS DFMC receiver, the MP-free C/N_0 degradation model proposed in [1] as well as two important notions: the pulse independency condition and the BIA, are introduced and applied to the DME/TACAN MP-free RFI signal.

Generic airborne GNSS DFMC receiver: In order to understand the MP-free C/N_0 degradation model, first a generic airborne GNSS DFMC receiver, as well as a description of its components behavior and effect on the received useful and RFI signals are provided. The airborne GNSS DFMC generic structure block scheme is provided in Fig. 1.

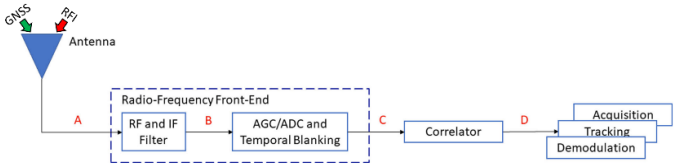

Fig. 1. Airborne GNSS DFMC generic receiver block scheme.

First, the antenna is in charge of capturing all the in-band incoming signals, which is a mix of useful GNSS signals and RFI signals. At the antenna port, the received signal at point A of Fig. 1 is passed to the RFFE block.

Multiple operations are performed in the RFFE block. First, the received signals are amplified, shifted from their original carrier frequency to a lower intermediate frequency and filtered to obtain the signal at point B of Fig. 1. The resulting signal is then digitalized by an Analog to Digital Converter (ADC) coupled with the Automatic Gain Controller (AGC), which is responsible for minimizing the losses brought by the quantization [21]. It is at this point that the temporal blanker is introduced [1].

The temporal blanker is the counter-measure selected by civil aviation standards to mitigate the pulsed RFI impact such as DME/TACAN or JTIDS/MIDS signals. Note that the final implementation depends on the receiver manufacturer since the temporal blanker exact structure is not standardized; three possible blanker implementations are provided in [12]. The temporal blanker is a device which blanks (puts to 0) the I/Q time samples of the incoming signal (mix of signals) which have an instantaneous power envelope over a given threshold, T_H. The instantaneous power envelope, $P_m(t)$, of a single Gaussian pulse generated by beacon m is defined as

$$P_m(t) = \mathrm{PEP}_m |g(t)|^2 = \mathrm{PEP}_m e^{-\alpha t^2}. \quad (7)$$

Note that for an optimal functioning of the GNSS receiver, AGC and temporal blanker must be coupled. Fig. 2 illustrates the instantaneous blanker application as defined in [1], where the blanking threshold is expressed in volts (V).

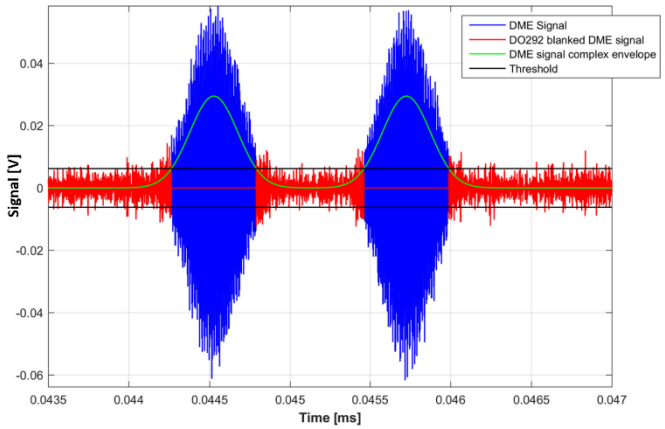

Fig. 2. Illustration of the RTCA DO-292 instantaneous blanker behavior over the DME signal.

At the RFFE block output, the digitized and blanked mix of GNSS and RFI signals at point C is fed to the correlator which multiplies the signal by two local replicas (the cosine and the incoming code), and coherently accumulates the resulting signal for T_{i} seconds, where T_{i} is the coherent integration time. At the output of the GNSS DMFC correlator (point D of Fig. 1), the basic operations of the GNSS receiver, i.e., the acquisition, tracking and demodulation of the GNSS signals are performed.

Note that, in the context of civil aviation, the GNSS signal C/N_0 must exceed a particular C/N_0 threshold to guarantee that the minimum requirements as defined in [22] on the acquisition, tracking and demodulation are met. The acquisition, tracking and demodulation C/N_0 thresholds are derived in [3],[23] and [4], respectively.

However, the GNSS signal C/N_0 is degraded by the presence of RFI signals and by the blanking mechanism. Therefore, a mathematical model of the C/N_0 degradation must be derived to ensure that, even in presence of RFI, the GNSS C/N_0 still exceeds the C/N_0 threshold.

General C/N_0 degradation model: The chosen figure of merit to measure the impact of the RFI signals and the blanking method on the GNSS signal C/N_0 is the effective C/N_0, $C/N_{0,\mathrm{eff}}$. $N_{0,\mathrm{eff}}$ represents the effective noise power spectrum density that a receiver will observe at the antenna port which generates the same power at the GNSS DFMC correlator output as the power generated by the nominal noise with PSD equal to N_0 plus the power generated by the analyzed interferences, when assuming that all RFFE elements and the correlator are ideal, and that no blanker is implemented.

The derivation of $C/N_{0,\mathrm{eff}}$ is based on a computation of the Signal to Noise plus Interference Power Ratio (SNIR) at the GNSS DFMC correlator output (point D of Fig. 1). The complete calculation of the SNIR in presence of the temporal blanker and pulsed interferences is provided in [9],[13] and, from this derivation, $C/N_{0,\mathrm{eff}}$ is simply retrieved by dividing the SNIR by $4T_I$. Under this rationale, the mathematical model for $N_{0,\mathrm{eff}}$ in presence of pulsed RFI for a receiver implementing a temporal blanker is [1],[9],[13]

$$N_{0,\mathrm{eff}} = \frac{N_O}{1-\mathrm{bdc}} \cdot \left(1 + \frac{I_{0,\mathrm{WB}}}{N_0} + R_{\mathrm{I}}\right), \tag{8}$$

where N_0 is the thermal noise power spectrum density, bdc is the blanker duty cycle which represents the percentage of time the RFI signals trigger the blanker, $I_{0,WB}$ is the equivalent white noise contribution of wideband (non-pulsed) RFI and R_{I} is the below-threshold interfering-signal-to-thermal-noise ratio which represents the contribution of the RFI signals unblanked part. Further discussion about this model can be found in [13].

The difference between the C/N_0 when only the useful signal is present, $C/N_{0,\mathrm{nom}}$, and the C/N_0 when the useful signal and the RFI are present, $C/N_{0,\mathrm{eff}}$, is called the C/N_0 degradation. In the framework of this manuscript, DME/TACAN are assumed to be the only RFI present at the antenna port and therefore $I_{0,\mathrm{WB}} = 0$. Finally, since bdc and R_{I} are equal to zero when no RFI is present ($N_{0,\mathrm{nom}} = N_0$), the C/N_0 degradation in dB is expressed as

$$\left(\frac{C}{N_0}\right)_{\mathrm{deg}} = 10\log_{10}\left(\frac{N_{0,\mathrm{eff}}^{\mathrm{RFI}}}{N_{0,\mathrm{nom}}}\right) = 10\log_{10}\left(\frac{1-\mathrm{bdc}}{1+R_{\mathrm{I}}}\right). \tag{9}$$

The definition of bdc and R_{I} assuming only DME/TACAN and without MP are based on two important notions presented next.

Pulse independency condition (PIC): In this work, the PIC is said to be fulfilled when the power of the summation of the N pulses is equal to the sum of the individual powers of each pulse, i.e.,

$$\Upsilon\left(\sum_{n=1}^{N} p_n(t)\right) = \sum_{n=1}^{N} \Upsilon\left(p_n(t)\right), \tag{10}$$

where $\Upsilon(X)$ denotes the power of X and $p_n(t)$ is the temporal expression of pulse n, $n \in [\![1, N]\!]$. In the remaining part of the article, if no set of N pulses is specified for the PIC then it applies to any pulse irrespective of the source, emission and composite pulse.

Blanker independency assumption (BIA): Under the PIC, the triggering of the temporal blanker by pulse n is assumed to be independent from the triggering of any other pulse $n', n' \neq n$ coming from other source or even the same source by [1].

The MP-free C/N_0 degradation model proposed in [1] aims at providing a statistical average of the C/N_0 degradation generated by DME/TACAN for a single aircraft position. Therefore, the time of observation T_0 representing the time when the aircraft is in the same position is assumed to be very short ($T_0 \to 0$). Consequently, inside $t \in [0, T_0]$, since $T_0 \ll T_D$, propagation time delay is approximated as $\tau_m(t) \approx \tau_m(0)$. In the remaining part of the paper, τ_m is used as an abusive notation for $\tau_m(0)$.

At the aircraft chosen position, the additional phase offset due to the propagation channel physical effects $\theta_{\mathrm{e},m}$ is assumed by [1] to be unknown and thus $\theta_{\mathrm{e,m}}$ is modelled as a uniform

variable over $[0,2\pi)$ independent for $m \neq m'$ (since the DME/TACAN beacons are not located at the same location). In other words, the C/N_0 degradation is derived by averaging all the possible additional phase outcomes in $[0,2\pi)$. Therefore, the modelling of the three random variables t_m^κ, $\theta_{0,m}^\kappa$ and $\theta_{\mathrm{e},m}$ of the received signal $v(t)$ assumed by [1] is

$$\begin{aligned} t_m^\kappa &\sim U[0,T_0],\ t_m^\kappa \perp \theta_m^{\kappa'},\ \forall\, m,m',\kappa,\kappa', \\ \theta_{0,m}^\kappa &\sim U[0,2\pi),\ \theta_{0,m}^\kappa \perp \theta_{0,m'}^{\kappa'},\ \forall \binom{m}{\kappa} \neq \binom{m'}{\kappa'}, \\ \theta_{\mathrm{e},m} &\sim U[0,2\pi),\ \theta_{\mathrm{e},m} \perp \theta_{\mathrm{e},m'},\ \forall m \neq m', \\ \theta_{\mathrm{e},m} &\perp \theta_{0,m'}^{\kappa}\ \forall\, m,m',\kappa. \end{aligned} \tag{11}$$

where $\binom{m}{\kappa} \neq \binom{m'}{\kappa'}$ means that at least $m \neq m'$ or $\kappa \neq \kappa'$ and $\perp$ means independent. This modelling of t_m^κ and θ_m^κ is referred as the statistical assumption in this article.

Under the statistical assumption (11), the PIC is fulfilled (see Section III.B) and therefore the BIA applies. The MP-free modelling of R_I and bdc under the BIA is provided next.

Multipath-free DME/TACAN bdc mathematical model: In this section, bdc, $\mathrm{pw}_m^{\mathrm{eq}}$, $I_{\mathrm{bdc},m}$, l_m and r_m are defined and illustrated in Fig. 3 for an above-threshold composite pulse (two Gaussian pulses in the MP-free case). Note that the definition of $\mathrm{pw}_m^{\mathrm{eq}}$ is particularly important since its model will be updated with the introduction of MP.

Under the BIA, the DO-292 models the MP-free DME/TACAN bdc mathematical model is based on Queueing Theory [24] as [8],

$$\mathrm{bdc} = 1 - e^{-\sum_{m=1}^{M} \mathrm{pw}_m^{\mathrm{eq}} \mathrm{PRF}_m}, \tag{12}$$

where $\mathrm{pw}_m^{\mathrm{eq}}$ is the above blanker width generated by any received composite pulse κ_0 in $[\![1,\mathrm{K}_m]\!]$ of source m.

An important property of $\mathrm{pw}_m^{\mathrm{eq}}$ is that it is invariant by translation, i.e., the delay of the first received pulse of the composite pulse, $t_m^{\kappa_0} + \tau_m$, does not matter. It is thus chosen at 0 to simplify the derivation as represented in Fig. 3. In that case $\mathrm{pw}_m^{\mathrm{eq}}$ is expressed as

$$\mathrm{pw}_m^{\mathrm{eq}} = \mu\left(I_{\mathrm{bdc},m}\right), \tag{13}$$

where $I_{\mathrm{bdc},m}$ is the blanked interval generated by the received composite pulse κ_0 and μ is the unidimensional Lebesgue measure, i.e., $\mu([a,b]) = b - a$. Since the composite pulse is composed of two disjoint Gaussian pulses in the MP-free case (1), $I_{\mathrm{bdc},m}$ is decomposed in two disjoint blanked intervals as

$$I_{\mathrm{bdc},m} = I_{\mathrm{bdc},m}^0 \bigsqcup I_{\mathrm{bdc},m}^1, \tag{14}$$

where $I_{\mathrm{bdc},m}^0$ and $I_{\mathrm{bdc},m}^1$ are the blanked intervals generated by the first and the second pair of the composite pulse, respectively. The blanked intervals generated by the first pulse $I_{\mathrm{bdc},m}^0$ are mathematically expressed as

$$I_{\mathrm{bdc},m}^0 = \begin{cases} \{\emptyset\} \text{ if } \mathrm{PEP}_m \leq \mathrm{T_H} \\ [\mathrm{l}_m^0, \mathrm{r}_m^0] \text{ otherwise,} \end{cases} \tag{15}$$

where $\mathrm{T_H}$ is the blanking threshold and l_m^0 and r_m^0 respectively are the instants of time when the pulse starts and stops to be blanked. Assume that $\mathrm{PEP}_m > \mathrm{T_H}$, the mathematical expression of l_m^0 and r_m^0 is obtained by equalizing the instantaneous peak power envelope (7) of the first pulse, $P_m(t)$ to $\mathrm{T_H}$, i.e.,

$$\begin{aligned} P_m(t) = \mathrm{T_H} &\Leftrightarrow \begin{cases} \mathrm{l}_m^0 = -w_m \\ \mathrm{r}_m^0 = w_m, \end{cases} \\ w_m &= \sqrt{\ln\left(\frac{\mathrm{PEP}_m}{\mathrm{T_H}}\right)/\alpha} \end{aligned} \tag{16}$$

and thus $I_{\mathrm{bdc},m}^0 = [-w_m, w_m]$. The blanked interval $I_{\mathrm{bdc},m}^1$ is obtained by applying exactly the same methodology but to a pulse delayed by Δt and thus $I_{\mathrm{bdc},m}^1 = [\Delta t - w_m, \Delta t + w_m]$. Finally, in the MP-free case, $\mathrm{pw}_m^{\mathrm{eq}}$ is given from (13), using the σ-additivity of the Lebesgue measure,

$$\mathrm{pw}_m^{\mathrm{eq}} = \mu\left(I_{\mathrm{bdc},m}^0\right) + \mu\left(I_{\mathrm{bdc},m}^1\right) = 4w_m \tag{17}$$

which concludes the derivation of bdc in the MP-free case.

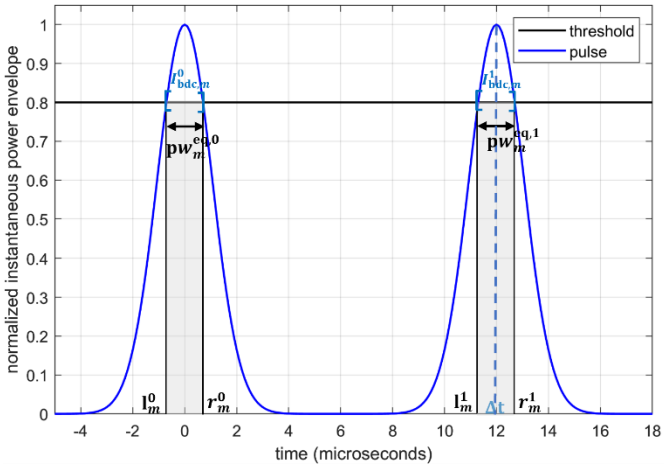

Fig. 3. Graphical illustration of $\mathrm{pw}_m^{\mathrm{eq}}$, $I_{\mathrm{bdc},m}$, l_m and r_m parameters for an above-threshold composite pulse in the MP-free case.

Multipath-free DME/TACAN R_I mathematical model: Under the BIA, the MP-free mathematical model of R_I as proposed by [25] is given by

$$R_\mathrm{I} = \sum_{m=1}^{M} \frac{P_{\mathrm{r},m}}{N_0 \beta_0} \cdot \mathrm{SSC}(\Delta f_m), \tag{18}$$

where β_0 is the thermal noise power degradation due to RFFE filter and GNSS DMFC correlator, $\mathrm{SSC}(\Delta f_i)$ is the Spectral Separation Coefficient of the pulsed interfering source m as expressed in [13] and $P_{\mathrm{r},m}$ is the post-blanker average power of the received RFI signal coming from beacon m assuming that the blanker has been triggered by beacon m only [1]. This last term is of particular importance since it can be decomposed to define a new quantity $\mathrm{PW}_m^{\mathrm{eq}}$ as

$$P_{\mathrm{r},m} \quad = \quad \mathrm{PEP}_m \mathrm{PW}_m^{\mathrm{eq}} \mathrm{PRF}_m, \tag{19}$$

where $\mathrm{PW}_m^{\mathrm{eq}}$ is the width of a rectangular pulse with amplitude PEP_m and same energy as any post-blanker received composite pulse κ_0 in $[\![1, \mathrm{K}_m]\!]$ of source m. As for $\mathrm{pw}_m^{\mathrm{eq}}$, $\mathrm{PW}_m^{\mathrm{eq}}$ is translation invariant, and therefore $t_m^{\kappa_0} + \tau_m$ is chosen at 0 to simplify the derivation.

Since PIC is fulfilled, $\mathrm{PW}_m^{\mathrm{eq}}$ is modelled by [1] as

$$\mathrm{PW}_m^{\mathrm{eq}} \quad = \quad \mathrm{PW}_m^{\mathrm{eq},0} + \mathrm{PW}_m^{\mathrm{eq},1}, \tag{20}$$

where $\mathrm{PW}_m^{\mathrm{eq},0}$ and $\mathrm{PW}_m^{\mathrm{eq},1}$ are the equivalent pulse widths of the first and the second pulse of the received composite pulse, respectively.

With this definition, $\mathrm{PW}_m^{\mathrm{eq},0}$ and $\mathrm{PW}_m^{\mathrm{eq},1}$ are obtained by equalizing the energy of the first and the second pulse of the composite pulse to a rectangular pulse whose amplitude is PEP_m, i.e., from (7),

$$\begin{aligned} \mathrm{PW}_m^{\mathrm{eq},0} &= \frac{1}{\mathrm{PEP}_m} \int_{\mathbb{R}} P_m(t) b_m(t) dt \\ \mathrm{PW}_m^{\mathrm{eq},1} &= \frac{1}{\mathrm{PEP}_m} \int_{\mathbb{R}} P_m(t - \Delta t) b_m(t) dt. \end{aligned} \tag{21}$$

In (21), $b_m(t)$ represents the temporal blanker generated by the received composite pulse under the BIA. Following the RTCA DO-292 blanker model [1], $b_m(t)$ is expressed as, from (14),

$$b_m(t) = \begin{cases} 0 \text{ if } t \in I_{bdc,m} \\ 1 \text{ otherwise} \end{cases} \tag{22}$$

Note that $b_m(t)$ is an artificial signal since only one DME/TACAN source is considered to trigger the blanker, whereas in reality, all sources can trigger the blanker [13]. Nevertheless, the impact of the other sources has already been accounted for in (18) and is approximated to $(1 - bdc)$ [13].

Using $I_{bdc,m}$ expression (14) and assuming that the blanked interval $I_{\mathrm{bdc},m}^0$ ($I_{\mathrm{bdc},m}^1$) generated by the first (second) pulse impact on the second (first) pulse is negligible given the 12 µs separation [1], $e^{-\alpha \Delta t^2} \ll 1$, $\mathrm{PW}_m^{\mathrm{eq},0}$ and $\mathrm{PW}_m^{\mathrm{eq},1}$ are given by

$$\begin{aligned} \mathrm{PW}_m^{\mathrm{eq},0} &= \int_{\mathbb{R}} e^{-\alpha t^2} dt - \int_{t \in I_{\mathrm{bdc},m}^0} e^{-\alpha t^2} dt \\ \mathrm{PW}_m^{\mathrm{eq},1} &= \int_{\mathbb{R}} e^{-\alpha (t - \Delta t)^2} dt - \int_{t \in I_{\mathrm{bdc},m}^1} e^{-\alpha (t - \Delta t)^2} dt \end{aligned} \tag{23}$$

A closed-form solution of (23) can be found by considering the two following cases:

1. Received PEP of beacon m pulses are below-blanker. Then, $I_{\mathrm{bdc},m} = \{\emptyset\}$ and, by solving the Gaussian integral,

$$\begin{aligned} \mathrm{PW}_m^{\mathrm{eq},0} &= \int_{\mathbb{R}} e^{-\alpha t^2} dt = \sqrt{\pi/\alpha} \\ \mathrm{PW}_m^{\mathrm{eq},1} &= \int_{\mathbb{R}} e^{-\alpha (t - \Delta t)^2} dt = \sqrt{\pi/\alpha} \\ \mathrm{PW}_m^{\mathrm{eq}} &= \mathrm{PW}_m^{\mathrm{eq},0} + \mathrm{PW}_m^{\mathrm{eq},1} = 2\sqrt{\pi/\alpha} \end{aligned} \tag{24}$$

2. Received PEP of beacon m pulses are above-blanker. Then $\mathrm{PW}_m^{\mathrm{pulse}}$ is given by

$$\begin{aligned} \mathrm{PW}_m^{\mathrm{eq},0} &= \int_{\mathbb{R}} e^{-\alpha t^2} dt - \int_{\mathrm{l}_m^0}^{\mathrm{r}_m^0} e^{-\alpha t^2} dt \\ &= \sqrt{\frac{\pi}{\alpha}} \mathrm{erfc}\left(\sqrt{\alpha} w_m\right), \\ \mathrm{PW}_m^{\mathrm{eq},1} &= \int_{\mathbb{R}} e^{-\alpha (t - \Delta t)^2} dt - \int_{\mathrm{l}_m^1}^{\mathrm{r}_m^1} e^{-\alpha (t - \Delta t)^2} dt \\ &= \sqrt{\frac{\pi}{\alpha}} \mathrm{erfc}\left(\sqrt{\alpha} w_m\right), \\ \mathrm{PW}_m^{\mathrm{eq}} &= \mathrm{PW}_m^{\mathrm{eq}} + \mathrm{PW}_m^{\mathrm{eq}} = 2\sqrt{\frac{\pi}{\alpha}} \mathrm{erfc}\left(\sqrt{\alpha} w_m\right), \end{aligned} \tag{25}$$

where erfc is the complementary error function,

$$\mathrm{erfc}(x) = \frac{2}{\sqrt{\pi}} \int_x^{\infty} e^{-t^2} dt\,. \tag{26}$$

From the definition of R_{I}, $\mathrm{PW}_m^{\mathrm{eq}}$ is the most important parameter as it must be updated with the MP introduction.

Note that R_{I} definition (18) provided in this paper slightly differs from the one proposed in [1]. This is because the post-blanker RFI power spectrum density (PSD) used in the SSC term is assumed not to be perfectly spread as it is shown in [13], better modelling R_{I}, contrary to the assumption of [1]. However, since the only modification assumed in this paper by the introduction of MP is for the formula of $\mathrm{PW}_m^{\mathrm{eq}}$, both models from [1] and [13] are modified in the same manner.

III. STATISTICAL C/N_0 DEGRADATION MODEL CONSIDERING MULTIPATH

In this section, the current MP-free statistical C/N_0 degradation model is updated to account for echoes generated by scatterers in the Radio Line Of Sight (RLOS) of the DME/TACAN beacons. The proposed model aims at providing an average statistical value of the C/N_0 degradation for a single point of an aircraft trajectory. The MP collisions are tackled by the model and the models of $\mathrm{PW}^{\mathrm{eq}}$ (and thus R_I) and $\mathrm{pw}^{\mathrm{eq}}$ (and thus bdc) are updated to accurately consider MP. Note that the terms "echo" and "MP" are used interchangeably to designate multipath. Finally, note that the statistical C/N_0 degradation model considering multipath is a low complex model which is derived to be used for RFI environment analysis with a large number of scatterers.

A. Modelling of The Multipath Parameters

In this work, the MP are characterized by 5 parameters. First, there is the number of MP N_m generated by one DME/TACAN beacon m. Then, for each MP $n \in [1, N_m]$ it is possible to define its amplitude A_m^n, delay τ_m^n, Doppler frequency $f_{D,m}^n$ and additional phase $\theta_m^{\kappa,n}$.

While the parameters N_m, A_m^n and τ_m^n usually exhibit strong stochastic characteristics, they are assumed in this work to be the outputs of the air-ground propagation channel developed in Part II [16]. As such, they are assumed to be deterministic in this work. Furthermore, even if the Doppler frequency $f_{D,m}^n$ is not provided by the proposed air-ground propagation channel model, it is still assumed to be a deterministic parameter; its mathematical model is provided in (4). The reader is referred to Part II of this word for a more thorough explanation on the number, amplitude and additional delay N_m, A_m^n and τ_m^n of the MP [16].

Finally, the additional phase $\theta_m^{\kappa,n}$ is updated from (5) into

$$\theta_m^{\kappa,n} = \theta_{0,m}^{\kappa} + \theta_{\mathrm{D},m}^{n} + \theta_{\mathrm{e},m}^{n} \bmod 2\pi, \tag{27}$$

where $\theta_{\mathrm{D},m}^{n}$ is the additional phase due to initial propagation time delay of pulse n, i.e., $\theta_{\mathrm{D},m}^{n} = -2\pi f_m \tau_m^n$. Since MP are now considered, the additional phase offset $\theta_{\mathrm{e},m}^{n}$ introduced by any physical effects generated by the environment must now also account for reflections and thus not only the weather but also any time dependent properties of the scatterer (open windows, closed shutters, constructions, etc.) must be considered. Since MP are generated from different scatterers, $\theta_{\mathrm{e},m}^{n}$ now depends on n.

Note that the limitations of such modelling of the MP parameters is provided in Section III.F.

B. Received Signal Model Under the Statistical Assumption Considering Multipath

Considering MP, the main difference for the received signal is that the received composite pulse is no longer composed of one pair of pulses but of N_m pair of pulses, where $N_m \geq 1$ and N_m is the number of scatterers in the RLOS of the DME/TACAN beacon. Artificially imposing that composite pulses coming from a source m can only be blanked by themselves and not by the other sources $m' \neq m$ [1], the expression of the received signal at the output of the blanker (and not only at the output of the antenna) $r(t)$ is expressed as, still considering a single aircraft position,

$$r(t) = \sum_{m=1}^{M} \sum_{\kappa=1}^{\mathrm{K}_m} \sum_{n=0}^{N_m} A_m^n s_{\mathrm{bb}}(t - t_m^{\kappa} - \tau_m^n) \cdot \cos\left(2\pi\left(f_m + f_{D,m}^n\right)t + \theta_m^{\kappa,n}\right) b_m(t - t_m^{\kappa} - \tau_m^0), \tag{28}$$

where the index $n = 0$ is associated with the direct (LOS) composite pulse.

For this section (and this section only), it is more convenient to express each received composite pulse κ with the individual Gaussian pulses $g(t)$ provided in (1), considering that the second pulse of the MP-free composite pulse is also an echo. In that case, the received composite pulse is composed of $N_m^{\mathrm{p}} + 1$ Gaussian pulses where N_m^{p} is the number of echoed pulses, $N_m^{\mathrm{p}} = 2N_m + 1$. Under this rationale, $r(t)$ is expressed in its most concise manner as

$$r(t) = \sum_{m,\kappa,n} f(m,\kappa,n), \quad f(m,\kappa,n) = A_m^n g(t - t_m^{\kappa} - \tau_m^n) \cdot \cos\left(2\pi\left(f_m + f_{D,m}^n\right)t + \theta_m^{\kappa,n}\right) b_m(t - t_m^{\kappa} - \tau_m^0), \tag{29}$$

where $m \in [\![1, M]\!]$, $\kappa \in [\![1, \mathrm{K}_m]\!]$ and $n \in [\![0, N_m^p]\!]$. Note that, with this rationale, there always exists an n such that $\tau_m^n = \Delta t$.

The function $b_m(t)$ represents the temporal blanker triggered by a received composite pulse of beacon m. The function b_m is simply delayed to match with the time of reception of the composite pulses but is always the same: since only a single aircraft trajectory point is analyzed, the received composite pulse is always the same and so the additional delay of the echoes with respect to the LOS is the same no matter t_m^{κ}.

Furthermore, assuming a single point of an aircraft trajectory, environmental conditions and scatterers time dependent properties can be assumed unknown, and thus $\theta_{\mathrm{e},m}^{n}$ (27) is modelled as a uniform distribution over $[0,2\pi)$, independent for different beacons ($m \neq m'$) and, without loss of generality since $e^{-\alpha \Delta t^2} \ll 1$, scatterers ($n \neq n'$). This assumption is referred as the statistical assumption in this article.

To summarize, the three random variables of $r(t)$ are modelled as

$$\begin{aligned} t_m^{\kappa} &\sim U[0,T_0],\ t_m^{\kappa} \perp \theta_{m'}^{\kappa',n}\ \forall\, m,m',\kappa,\kappa',n, \\ \theta_{0,m}^{\kappa} &\sim U[0,2\pi),\ \theta_{0,m}^{\kappa} \perp \theta_{0,m'}^{\kappa'}\ \forall \binom{m}{\kappa} \neq \binom{m'}{\kappa'}, \\ \theta_{\mathrm{e},m}^{n} &\sim U[0,2\pi),\ \theta_{\mathrm{e},m}^{n} \perp \theta_{\mathrm{e},m'}^{n'},\ \forall \binom{m}{n} \neq \binom{m'}{n'}, \\ \theta_{\mathrm{e},m}^{n} &\perp \theta_{0,m'}^{\kappa}\ \forall\, m,m',\kappa,n. \end{aligned} \tag{30}$$

C. Average Power of the Received Signal at Blanker Output

In order to derive $P_{\mathrm{r,m}}^{\mathrm{s}}$ from (18), the average post-blanker (where only beacon m can trigger the blanker) power of the composite pulses received from a source m under the statistical assumption, it is necessary to derive the average power P_{r}^{s} of the post blanker received signal $r(t)$. As a random and real signal, the average received power P_{r}^{s} of $r(t)$ under the statistical assumption is given by

$$P_{\mathrm{r}}^{s} = \lim_{T\to\infty} \frac{1}{2T} \int_{-T}^{T} E[r(t)^2]dt. \tag{31}$$

Note that in the integral of (31), a change in the value of t does not represent a change of the aircraft position (the aircraft is always fixed to one position), but rather the time period $[-T,T]$ when the aircraft is able to be in the analyzed fixed position of the trajectory. The integral must thus divide its result by $2T$ to get an average value. Moreover, since all instants of time are possible and thus are inspected, the analyzed time period tends to the infinite, ($T \to \infty$).

The expectation $E[r(t)^2]$ can be expressed as, from (29),

$$\begin{aligned} E[r(t)^2] &= E\left[\left(\sum_{m,\kappa,n} f(m,\kappa,n)\right)^2\right] \\ &= \sum_{m,m',\kappa,\kappa',n,n'} E[f(m,\kappa,n)f(m',\kappa',n')] \end{aligned} \tag{32}$$

by the linearity of the expectation. Let E_f be $E[f(m,\kappa,n)f(m',\kappa',n')]$. Then, since $t_m^{\kappa} \perp \theta_m^{\kappa,n}$,

$$E_f = A_m^n A_{m'}^{n'} E_g^{\mathrm{b}} E_{\cos} \tag{33}$$

where

$$\begin{aligned} E_g^{\mathrm{b}} &= E[g(t-t_m^{\kappa}-\tau_m^n)g\left(t-t_{m'}^{\kappa'}-\tau_{m'}^{n'}\right)\cdot \\ &\quad b_m\left(t-t_m^{\kappa}-\tau_m^0\right)b_{m'}(t-t_{m'}^{\kappa'}-\tau_{m'}^0)] \\ E_{\cos} &= E[\cos\left(2\pi\left(f_m+f_{D,m}^n\right)t+\theta_m^{\kappa,n}\right)\cdot \\ &\quad \cos\left(2\pi\left(f_{m'}+f_{D,m'}^{n'}\right)t+\theta_{m'}^{\kappa',n'}\right)] \end{aligned} \tag{34}$$

The value of E_f is investigated regarding the triplets (m,κ,n) and (m',κ',n'):

1. Assume emitting sources to be different, i.e., $m \neq m'$ then $\theta_{0,m}^{\kappa} \perp \theta_{0,m'}^{\kappa'}$, $\theta_{\mathrm{e},m}^{n} \perp \theta_{\mathrm{e},m'}^{n'}$ and thus $E_{\cos}$ can be separated into two expectations that both equal 0 by the law of total expectation since $\theta_{0,m}^{\kappa}$ and $\theta_{\mathrm{r},m}^{n}$ are uniform on $[0,2\pi)$. Thus, if $m \neq m'$ then $E_f = 0$.
2. Assume emitting sources are the same ($m = m'$) but emitted pulses come from different pairs, i.e., $\kappa \neq \kappa'$. Then, if $n = n'$, the product of the two gaussian pulses in E_g^{b} is assumed to be zero since pulse pairs are at least separated by 60 µs as specified in [19]. If $n \neq n'$, the product of the two gaussian pulses is still zero since MP having an additional delay close to 60 µs are expected to have an extremely small PEP (see numerical results in [16]). Therefore, if $m = m'$ and $\kappa \neq \kappa'$ then $E_f = 0$.
3. Assume emitted pairs of the same emitting source ($m = m'$ and $\kappa = \kappa'$) but different echoes, i.e., $n \neq n'$ then $\theta_{\mathrm{e},m}^{n} \perp \theta_{\mathrm{e},m}^{n'}$ and by the law of total expectation, assuming $\theta_{0,m}^{\kappa}$ known, $E_{\cos} = 0$ since $\theta_{\mathrm{e},m}^{n}$ and $\theta_{\mathrm{e},m}^{n'} \sim U[0,2\pi)$. Thus, if $m = m'$, $\kappa = \kappa'$ and $n \neq n'$ then $E_f = 0$.

To conclude, E_f is not zero only if $m = m'$, $\kappa = \kappa'$ and $n = n'$. Thus,

$$P_{\mathrm{r}}^{s} = \lim_{T\to\infty} \frac{1}{2T} \int_{-T}^{T} \sum_{m,\kappa,n} E[f(m,\kappa,n)^2]dt\,. \tag{35}$$

The complete derivation of (35) is conducted in Appendix A. The final expression of $P_{\mathrm{r},m}^{\mathrm{s}}$ is obtained from P_{r}^{s} by identification as

$$\begin{aligned} P_{\mathrm{r}}^{s} &= \sum_m P_{\mathrm{r},m}^{\mathrm{s}} \\ P_{\mathrm{r},m}^{\mathrm{s}} &= \mathrm{PRF_m} \sum_n \mathrm{PEP}_m^n \int_{-\infty}^{\infty} e^{-\alpha(u-\tau_m^n)^2} b_m(u-\tau_m^0)du \end{aligned} \tag{36}$$

Finally, from (36), the power of the summation of all the received pulses is equal to the summation of the power of all the individual pulses and thus under the statistical assumption, the PIC as presented in Section II.B is fulfilled. Therefore, the BIA as presented in Section II.B applies and the definition of $r(t)$ with $b_m(t)$ is justified for the purposes of calculating $P_{\mathrm{r},m}^{\mathrm{s}}$; note that the introduction of $b_m(t)$ does not affect the fulfillment of the PIC but rather the exact expression of $P_{\mathrm{r},m}^{\mathrm{s}}$ as seen in (36).The derivation of $\mathrm{pw}_m^{\mathrm{eq}}$ and $\mathrm{PW}_m^{\mathrm{eq}}$ considering MP under blanker independency is provided in Sections III.C and III.D, respectively.

D. $\mathrm{pw}_m^{\mathrm{eq}}$ Mathematical Model Considering Multipath

In this section, the mathematical expression of $\mathrm{pw}_m^{\mathrm{eq}}$ (13) under blanker independency is updated to accurately account for echoed pulses under the BIA.

With the introduction of echoes, the received composite pulse is no longer constituted of two disjoint Gaussian pulses but is composed of the LOS and the MP, that can potentially collide. Therefore, considering MP, $I_{\mathrm{bdc},m}$, the blanked interval generated by one received composite pulse must also account for the blanked intervals generated by the echoed pulses.

As for the MP-free case, $\mathrm{pw}_m^{\mathrm{eq}}$ is still invariant by translation, and therefore the delay of the first received pulse $t_m^{\kappa_0} + \tau_m^0$ can be chosen at 0 to simplify the derivations. Fig. 4 provides a graphical example of the blanked intervals generated by a direct pulse (in red) received at $t_m^{\kappa} + \tau_m^0 = 0$ and an echoed pulse (in green) above-threshold, where the blanked interval generated by the echo must clearly be accounted for.

Therefore, in presence of echoes, $I_{\mathrm{bdc},m}$ is updated from (14) into

$$I_{\mathrm{bdc},m} = \bigcup_{n=0}^{N_m^{\mathrm{p}}} I_{\mathrm{bdc},m}^n \,, \tag{37}$$

where $I_{\mathrm{bdc},m}^n$ is the blanked interval generated by echo n and is expressed as

$$I_{\mathrm{bdc},m}^n = \begin{cases} \{\emptyset\} \text{ if } \mathrm{PEP}_m^n \leq \mathrm{T_H} \\ [\mathrm{l}_m^n, \mathrm{r}_m^n] \text{ otherwise,} \end{cases}$$
$$\begin{cases} \mathrm{l}_m^n = \tau_m^n - w_m^n \\ \mathrm{r}_m^n = \tau_m^n + w_m^n, \end{cases} \tag{38}$$
$$w_m^n = \sqrt{\ln\left(\frac{\mathrm{PEP}_m^n}{\mathrm{T_H}}\right)/\alpha},$$

where $\mathrm{PEP}_m^n = (A_m^n)^2/2$ is the PEP of echo n with respect to beacon m. Note that equation (37) is only valid in case of the BIA (and thus is only valid if pulse independency is fulfilled). If blanker independency was not assumed, the sum of the individual pulses should first be derived and then $I_{\mathrm{bdc},m}$ could be calculated.

Furthermore, it is more convenient to express $\mathrm{pw}_m^{\mathrm{eq}}$ only with disjoint blanked intervals since some $I_{\mathrm{bdc},m}^n$ may overlap. Let $B_{\mathrm{d},m}^q$ be the disjoint blanked intervals and Q_m the number of disjoint blanked intervals generated by source m, then

$$\begin{aligned} I_{\mathrm{bdc},m} &= \coprod_{q=1}^{Q_m} B_{\mathrm{d},m}^q \\ B_{\mathrm{d},m}^q &= [\mathrm{l}_{\mathrm{d},m}^q, \mathrm{r}_{\mathrm{d},m}^q]. \end{aligned} \tag{39}$$

The bounds $\mathrm{l}_{\mathrm{d},m}^q$ and $\mathrm{r}_{\mathrm{d},m}^q$ of $B_{\mathrm{d},m}$ can be retrieved recursively using $I_{\mathrm{bdc},m}^n$, ordering the l_m^n such that $\mathrm{l}_m^n \leq \mathrm{l}_m^{n+1}$, as:

$$\begin{aligned} \mathrm{l}_{\mathrm{d},m}^1 &= \mathrm{l}_m^1, \\ \mathrm{r}_{\mathrm{d},m}^1 &= \mathrm{comp}\left(\mathrm{r}_m^1, \mathrm{l}_m^2\right), \\ \mathrm{l}_{\mathrm{d},m}^q &= \min_n \left(\mathrm{l}_m^n | \mathrm{l}_m^n > \mathrm{l}_{\mathrm{d},m}^{q-1}\right), q \geq 1, \\ n_q &= \arg\left(\min_n \left(\mathrm{l}_m^n | \mathrm{l}_m^n > \mathrm{l}_{\mathrm{d},m}^{q-1}\right)\right), q \geq 1, \\ \mathrm{r}_{\mathrm{d},m}^q &= \mathrm{comp}\left(\mathrm{r}_m^{n_q}, \mathrm{l}_m^{n_q+1}\right), \end{aligned} \tag{40}$$

$$\mathrm{comp}\left(\mathrm{r}_m^n, \mathrm{l}_m^{n+1}\right) = \begin{cases} \mathrm{r}_m^n \text{ if } \mathrm{r}_m^n \leq \mathrm{l}_m^{n+1} \\ \mathrm{comp}\left(\max(\mathrm{r}_m^n, \mathrm{r}_m^{n+1}), \mathrm{l}_m^{n+2}\right) \text{ otherwise.} \end{cases}$$

Finally, under the statistical assumption, $\mathrm{pw}_m^{\mathrm{eq}}$ is updated in presence of MP into, from (17) and by the σ-additivity of μ,

$$\begin{aligned} \mathrm{pw}_m^{\mathrm{eq}} &= \mu\left(\coprod_{q=1}^{Q_m} B_{\mathrm{d},m}^q\right) \\ &= \sum_{q=1}^{Q_m} \mu\left(B_{\mathrm{d},m}^q\right) = \sum_{q=1}^{Q_m} \left(\mathrm{r}_{\mathrm{d},m}^q - \mathrm{l}_{\mathrm{d},m}^q\right). \end{aligned} \tag{41}$$

Therefore, in presence of MP, bdc from (12) is simply updated by using the expression (41) of $\mathrm{pw}_m^{\mathrm{eq}}$. Fig. 4 provides a graphical representation of the union of the overlapping $I_{\mathrm{bdc},m}^0$ and $I_{\mathrm{bdc},m}^1$ overlapping blanked intervals from the direct (in red) and the echoed pulses (in green), to generate one disjoint blanked interval $B_{\mathrm{d},m}^1$.

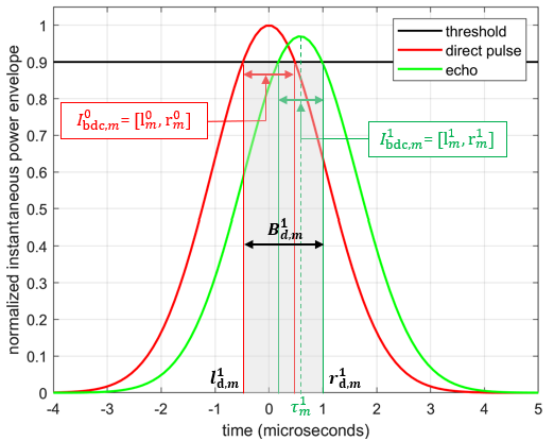

Fig. 4. Graphical representation of the overlapping blanked intervals generated by the direct pulse (in red) with an echoed pulse (in green) and the resulting disjoint blanked interval (in grey) at the output of the algorithm (40).

E. $\mathrm{PW}_m^{\mathrm{eq}}$ Mathematical Model Considering Multipath

In this subsection, the mathematical expressions of $\mathrm{PW}_m^{\mathrm{eq}}$ (20) under the BIA are updated to accurately account for

echoes. First, the expression of $\mathrm{PW}_m^{\mathrm{eq}}$ is provided based on the expression of the average post-blanker received power (36). Then, a closed-form of $\mathrm{PW}_m^{\mathrm{eq}}$ is obtained accounting for the three possible scenarios, by means of erfc functions.

Update of $\mathrm{PW}_m^{\mathrm{eq}}$ *considering multipath:* In presence of MP, the mathematical expression of $\mathrm{PW}_m^{\mathrm{eq}}$ is retrieved from (19) and from the expression of the average post blanker received power (36) as

$$\begin{aligned} P_{\mathrm{r},m}^{\mathrm{s}} &= \mathrm{PEP}_m^0 \mathrm{PW}_m^{eq} \mathrm{PRF}_m, \\ \mathrm{PW}_m^{eq} &= \sum_{n=0}^{N_m^{\mathrm{p}}} \frac{\mathrm{PEP}_m^n}{\mathrm{PEP}_m^0} \mathrm{PW}_m^{\mathrm{eq},n}. \end{aligned} \tag{42}$$

$\mathrm{PW}_m^{\mathrm{eq},n}$ is the equivalent pulse width which energy is the same as the energy of the post-blanker echo n relatively to beacon m, i.e.,

$$\mathrm{PW}_m^{\mathrm{eq},n} = \int_{-\infty}^{\infty} e^{-\alpha(t-\tau_m^n)^2} b_m(t-\tau_m^0)dt\,. \tag{43}$$

As for the MP-free case, $\mathrm{PW}_m^{\mathrm{eq},n}$ is translation invariant and therefore τ_m^0 can be chosen equal to 0. In that case $I_{\mathrm{bdc},m}$ in the MP case from (39) can be used and

$$\begin{aligned} \mathrm{PW}_m^{\mathrm{eq},n} &= \int_{\mathbb{R}} e^{-\alpha(t-\tau_m^n)^2} dt - \int_{t\in I_{\mathrm{bdc},m}} e^{-\alpha(t-\tau_m^n)^2} dt \\ &= \sqrt{\pi/\alpha} - \sum_{q}^{Q_m} J_m^{n,q}\,, \end{aligned} \tag{44}$$

as the $B_{\mathrm{d},m}^q$ are disjoints. Therefore, the integrals $J_m^{n,q}$ are expressed as

$$\begin{aligned} J_m^{n,q} &= \int_{t\in B_{\mathrm{d},m}^q} e^{-\alpha(t-\tau_m^n)^2} dt = \int_{\mathrm{l}_{\mathrm{d},m}^q}^{\mathrm{r}_{\mathrm{d},m}^q} e^{-\alpha(t-\tau_m^n)^2} dt \\ &= \int_{\mathrm{l}_{\mathrm{d},m}^q}^{\infty} e^{-\alpha(t-\tau_m^n)^2} dt - \int_{\mathrm{r}_{\mathrm{d},m}^q}^{\infty} e^{-\alpha(t-\tau_m^n)^2} dt \\ &= \frac{\sqrt{\pi/\alpha}}{2} \begin{pmatrix} \mathrm{erfc}\left(\sqrt{\alpha}\left(\mathrm{l}_{\mathrm{d},m}^q - \tau_m^n\right)\right) - \\ \mathrm{erfc}\left(\sqrt{\alpha}\left(\mathrm{r}_{\mathrm{d},m}^q - \tau_m^n\right)\right) \end{pmatrix}. \end{aligned} \tag{45}$$

The sign of $\mathrm{l}_{\mathrm{d},m}^q - \tau_m^n$ and $\mathrm{r}_{\mathrm{d},m}^q - \tau_m^n$ varies according to three possible scenarios that are detailed below.

Scenario 1: Echo n is being blanked by disjoint blanked interval q in its center, i.e., $\tau_m^n \in B_{\mathrm{d},m}^q$. A graphical representation of this scenario is provided in Fig. 5, where (red) inspected echo n is blanked at its center by the disjoint interval generated by, for example, another (green) echo.

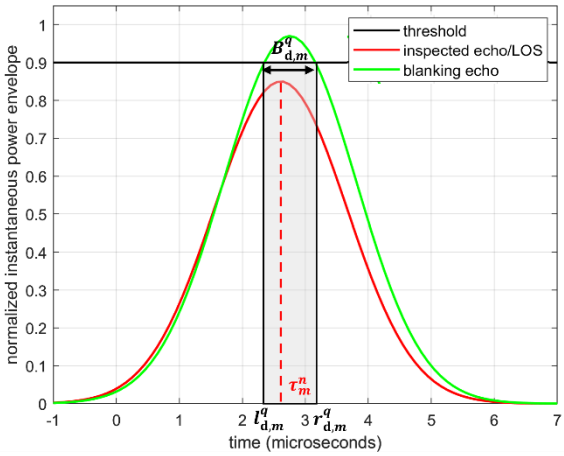

Fig. 5. Graphical representation of scenario 1: (red) echo n is being blanked at its center by the disjoint blanked interval generated by, for example, another (green) echo.

Note that this scenario differs from the MP-free case (25) since $B_{\mathrm{d},m}^q$ is not necessarily centered in t_m^κ. In that case, $\mathrm{l}_{\mathrm{d},m}^q - \tau_m^n \leq 0$ and $\mathrm{r}_{\mathrm{d},m}^q - \tau_m^n \geq 0$. Therefore, since $\mathrm{erfc}(-x) = 2 - \mathrm{erfc}(x)$, $J_m^{n,q}$ is expressed as, using the absolute value for convenience and from (45)

$$J_m^{n,q} = \frac{\sqrt{\pi/\alpha}}{2} \begin{pmatrix} 2 - \mathrm{erfc}\left(\sqrt{\alpha}\left|\mathrm{l}_{\mathrm{d},m}^q - \tau_m^n\right|\right) - \\ \mathrm{erfc}\left(\sqrt{\alpha}\left|\mathrm{r}_{\mathrm{d},m}^q - \tau_m^n\right|\right) \end{pmatrix}. \tag{46}$$

Scenario 2: Echo n is being blanked by disjoint blanked interval q on its left side, i.e., $\tau_m^n > r_{\mathrm{d},m}^q$. A graphical representation of this scenario is provided in Fig. 6, where (red) inspected echo n is blanked on its left side by the disjoint interval generated by another, for example, (green) echo.

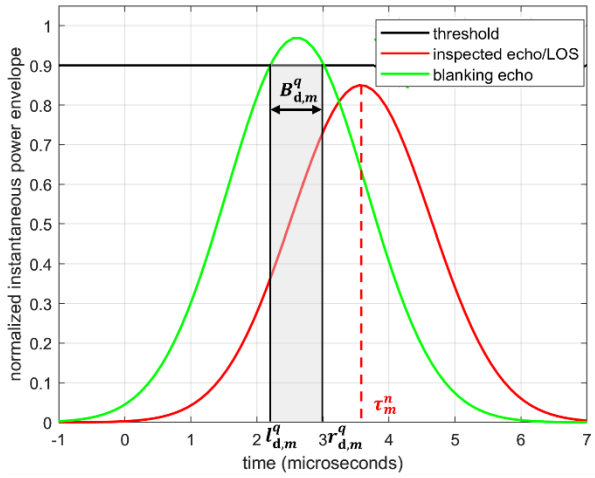

Fig. 6. Graphical representation of scenario 2: (red) echo n is being blanked by, for example, the disjoint blanked interval generated by another (green) echo on its left side.

In this scenario, $\mathrm{l}_{\mathrm{d},m}^{q} - \tau_m^n < 0$ and $\mathrm{r}_{\mathrm{d},m}^{q} - \tau_m^n < 0$. Therefore, in scenario 2,

$$J_m^{n,q} = \frac{\sqrt{\pi/\alpha}}{2}\begin{pmatrix}\mathrm{erfc}\left(\sqrt{\alpha}\left|\mathrm{r}_{\mathrm{d},m}^{q} - \tau_m^n\right|\right) - \\ \mathrm{erfc}\left(\sqrt{\alpha}\left|\mathrm{l}_{\mathrm{d},m}^{q} - \tau_m^n\right|\right)\end{pmatrix}. \tag{47}$$

Scenario 3: Echo n is being blanked by disjoint blanked interval q on its right side, i.e., $\tau_m^n < l_{\mathrm{d},m}^{q}$. A graphical representation of this scenario is provided in Fig. 7, where (red) inspected echo n is blanked on its right side by the disjoint interval generated by another, for example, (green) echo.

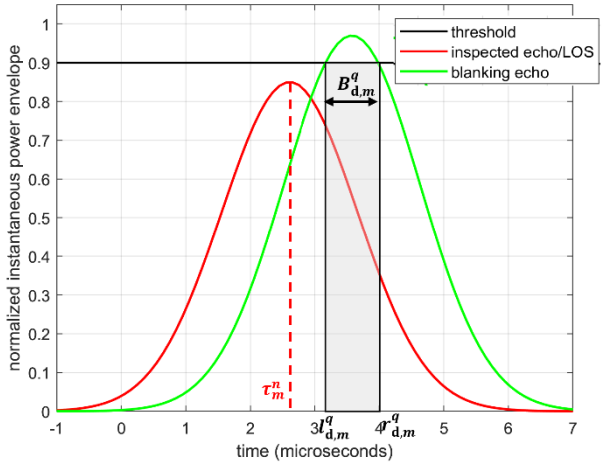

Fig. 7. Graphical representation of scenario 3: (red) echo n is being blanked by, for example, the disjoint blanked interval generated by another (green) echo on its right side.

In this scenario, $\mathrm{l}_{\mathrm{d},m}^{q} - \tau_m^n > 0$ and $\mathrm{r}_{\mathrm{d},m}^{q} - \tau_m^n > 0$. Therefore, in scenario 3,

$$J_m^{n,q} = \frac{\sqrt{\pi/\alpha}}{2}\begin{pmatrix}\mathrm{erfc}\left(\sqrt{\alpha}\left|\mathrm{l}_{\mathrm{d},m}^{q} - \tau_m^n\right|\right) - \\ \mathrm{erfc}\left(\sqrt{\alpha}\left|\mathrm{r}_{\mathrm{d},m}^{q} - \tau_m^n\right|\right)\end{pmatrix}. \tag{48}$$

Note that in Fig. 5, Fig. 6 and Fig. 7, the disjoint interval $B_{\mathrm{d},m}^{q}$ is only generated by one green echo for visualization purposes, and could be generated by any combination of more than one echo in reality.

The three formulas obtained for $J_m^{n,q}$ from the three scenarios can be reunited into one equation using the indicator $\mathbf{1}_E(x)$ and the $\mathrm{sign}(x)$ functions. In that case, $\mathrm{PW}_m^{\mathrm{eq,n}}$ from (44) is expressed as

$$\mathrm{PW}_m^{\mathrm{eq,n}} = \frac{\sqrt{\pi/\alpha}}{2}\left\{2 - \sum_{q=1}^{Q_m}\begin{bmatrix}2\cdot\mathbf{1}_{B_{\mathrm{d},m}^{q}}(\tau_m^n) - \\ \mathrm{sign}\left(\tau_m^n - l_{\mathrm{d},m}^{q}\right)\mathrm{erfc}\left(\sqrt{\alpha}\left|\mathrm{l}_{\mathrm{d},m}^{q} - \tau_m^n\right|\right) - \\ \mathrm{sign}\left(r_{\mathrm{d},m}^{q} - \tau_m^n\right)\mathrm{erfc}\left(\sqrt{\alpha}\left|r_{\mathrm{d},m}^{q} - \tau_m^n\right|\right)\end{bmatrix}\right\}. \tag{49}$$

Furthermore, since $\sum_{q=1}^{Q_m}\mathbf{1}_{B_{\mathrm{d},m}^{q}}(\tau_m^{\kappa,n}) = \mathbf{1}_{I_{\mathrm{bdc},m}}(\tau_m^n)$, the final expression of $\mathrm{PW}_m^{\mathrm{eq,n}}$ is given by

$$\mathrm{PW}_m^{\mathrm{eq,n}} = \frac{\sqrt{\pi/\alpha}}{2}\left\{2\left(1 - \mathbf{1}_{I_{\mathrm{bdc},m}^{\kappa}}(\tau_m^n)\right) + \sum_{q=1}^{Q_m}\begin{bmatrix}\mathrm{sign}\left(\tau_m^n - l_{\mathrm{d},m}^{q}\right)\mathrm{erfc}\left(\sqrt{\alpha}\left|\mathrm{l}_{\mathrm{d},m}^{q} - \tau_m^{\kappa,n}\right|\right) + \\ \mathrm{sign}\left(r_{\mathrm{d},m}^{q} - \tau_m^n\right)\mathrm{erfc}\left(\sqrt{\alpha}\left|\mathrm{r}_{\mathrm{d},m}^{q} - \tau_m^{\kappa,n}\right|\right)\end{bmatrix}\right\}. \tag{50}$$

R_{I} is thus updated in the presence of MP by using expression (50) of $\mathrm{PW}_m^{\mathrm{eq,n}}$ in (43). Note that formula (42), using (50), is validated by simulations in Section V.A.

Also note that it is assumed in this paper that even with the introduction of MP, SSC is the same for each received pulse (MP or LOS) in R_{I} (18). However, with the introduction of MP, SSC should not be the same across pulses, since the pulses are not blanked in the same manner. The study of the variations of SSC in the MP case is left for future work.

F. Model Necessary Inputs and Limitations

To compute bdc (12) and R_{I} (18) in presence of MP, only the values of $\mathrm{pw}_m^{\mathrm{eq}}$ (41) and $\mathrm{PW}_m^{\mathrm{eq}}$ (50) updated for the presence of MP under the statistical assumption, are necessary. To derive these quantities, the precise knowledge of the blanked interval $I_{\mathrm{bdc},m}$ (39) is mandatory. More specifically, the knowledge of the disjoint blanked intervals $B_{\mathrm{d},m}^{q}$ is required and thus, the values of all w_m^n (38) must be known. Therefore, the necessary inputs for the C/N_0 degradation model are the values of N_m and of all the additional delays τ_m^n and received PEP, PEP_m^n, in order to compute R_{I}, bdc (41) and finally the C/N_0 degradation (9) in presence of MP.

There are two limitations associated with the determination of deterministic values for N_m, τ_m^n and A_m^n. First, it requires an air-ground propagation channel model to be associated with a highly detailed scene to completely determine N_m and τ_m^n, and to limit the range of values of A_m^n (and potentially its probability density function). Second, since not all the uncertainty of A_m^n can be removed by the scene and the propagation channel model, a final selection of the value of A_m^n must be performed, which limits the representativity of the signal model; for example, the value A_m^n could be equal to the

statistical (or a worst-case statistical) mean limiting the signal representation to a mean amplitude signal; this choice is made in this two-part manuscript.

Part II of this work addresses these requirements by proposing a complete propagation channel model specifically designed to provide the values of N_m, τ_m^n and PEP_m^n for any MP generated by the scatterers in the RLOS of the visible DME/TACAN beacons [16].

IV. FIXED ENVIRONMENT C/N_0 DEGRADATION MODEL CONSIDERING MULTIPATH

In this section, the C/N_0 degradation model in presence of MP is investigated under the fixed environment assumption. This model provides an average statistical value of the C/N_0 degradation for a short aircraft trajectory under the condition that the channel propagation physical effects offset phase, θ_e, is known (a signal realization with respect to θ_e). Therefore, the proposed fixed environment C/N_0 degradation model considering multipath is a high complex model which is mainly derived to be used for RFI environments analysis with a low number of scatters and to verify the limits of the statistical environment. Thus, the analysis conducted in this section focuses on the additional calculations and limitations with respect to the statistical model.

The section is organized as follows. The fixed environment assumption is provided in Section IV.A. Section IV.B develops the average post-blanker received power under the fixed-environment assumption. Section IV.C discusses the PIC under the fixed environment assumption. Section IV.D mathematically defines the pulse independency zones where blanker independencies are evaluated. Finally, Section IV.E provides a summary comparison between the fixed environment model and the statistical model in terms of strengths and weaknesses, applicable scopes, and performance disparities.

A. Fixed Environment Assumption

The fixed environment assumption is defined as short periods of time T_0 (i.e., less than a second) during an aircraft trajectory where environmental conditions can be assumed to be constant. In other words, the phase offset produced by the physical effects generated by the environment, $\theta_{\mathrm{e},m}^n$, is assumed to have an initial unknown random value which remains constant for this short period of time; scatterers or the weather are unlikely to change during T_0.

Therefore, under the fixed environment assumption, $\theta_{\mathrm{e},m}^n$ is modelled as the addition of two terms, i.e.,

$$\theta_{\mathrm{e},m}^n = \theta_{\mathrm{e},m}^0 + \delta\theta_{\mathrm{e},m}^n. \tag{51}$$

In (51), $\theta_{e,m}^0$ is a first random term which follows a uniform distribution, $\theta_{e,m}^0 \sim U[0,2\pi)$ which models the unknown initial value of the pulses. The second term, $\delta\theta_{e,m}^n$, is deterministic and remains constant irrespective of the value of $\theta_{e,m}^0$ for each MP pulse n of the composite pulse. Note that keeping $\delta\theta_{e,m}^n$ constant irrespective of $\theta_{e,m}^0$ is the mathematical modelling proposed in this work to represent the analysis of a short segment of an aircraft trajectory $[0, T_0]$ where the environment conditions remain fixed once the initial unknown value, $\theta_{e,m}^0$, is randomly sampled.

Moreover, concerning the propagation delay, under the fixed environment assumption, for a fixed source m, the difference between two rays delays τ_m^n and $\tau_m^{n'}$, $n \neq n'$, $\Delta\tau_m^{n,n'} = \tau_m^n - \tau_m^{n'}$, is assumed to be constant over $[t, t+T_0]$ since T_0 is very short.

Therefore, the artificial post-blanker received signal $r(t)$ under the fixed environment assumption, defined by assuming that blanker impact on received signal from source m is only triggered by source m and not by any other sources $m' \neq m$, is defined as

$$\begin{aligned} r(t) &= \sum_{m,\kappa,n} f(m,\kappa,n)\,, \\ f(m,\kappa,n) &= A_m^n s_{\mathrm{bb}}(t - t_m^\kappa - \tau_m^n)\cdot \\ &\cos\left(2\pi\left(f_m + f_{D,m}^n\right)t + \theta_m^{\kappa,n}\right) b_m(t - t_m^\kappa - \tau_m^0), \end{aligned} \tag{52}$$

where s_{bb} is used in (52) for the received signal definition (instead of using the gaussian pulse g and considering the second pulse of the initial composite pulse (1) as an echo in (29)) and thus, the number of received MP is simply N_m. This approach simplifies the derivation of the average received power in this case. Furthermore, the random variables in (52) defined for the statistical assumption in (30) are updated for the environment fixed assumption into

$$\begin{aligned} t_m^\kappa &\sim U[0,T_0],\, t_m^\kappa \perp \theta_{m'}^{\kappa',n}\ \forall\, m,m',\kappa,\kappa',n, \\ \theta_{0,m}^\kappa &\sim U[0,2\pi),\, \theta_{0,m}^\kappa \perp \theta_{0,m'}^{\kappa'},\ \forall \binom{m}{\kappa} \neq \binom{m'}{\kappa'}, \\ \theta_{\mathrm{e},m}^n &\sim U[0,2\pi),\, \theta_{\mathrm{e},m}^0 \perp \theta_{\mathrm{e},m'}^0, \forall m \neq m', \\ \delta\theta_{\mathrm{e},m}^n &\in [0,2\pi) \end{aligned} \tag{53}$$

Note that, for simplification purposes, $\delta\theta_{\mathrm{e},m}^0$ is assumed to be equal to zero.

B. Average Received Power at The Blanker Output

The derivation of the average received power under the fixed environment assumption $P_{\mathrm{r}}^{\mathrm{f}}$ at the blanker output follows the exact same step as the derivation of P_{r}^{s} under the statistical assumption as provided in Section III.B. The main difference is that under the fixed environment assumption, the expectation $E_{\cos}$ is not zero when $n \neq n'$, since $\theta_{\mathrm{e},m}^n$ is not a random variable anymore (59) and therefore pulse independency is only fulfilled between sources and emissions but not in terms

of composite pulse. In that case, $P_{\mathrm{r}}^{\mathrm{f}}$ can be expressed with two terms $P_{\mathrm{r}}^{\mathrm{f,d}}$ and $P_{\mathrm{r}}^{\mathrm{f,c}}$ as

$$\begin{aligned} P_{\mathrm{r}}^{\mathrm{f}} &= P_{\mathrm{r}}^{\mathrm{f,d}} + P_{\mathrm{r}}^{\mathrm{f,c}}, \\ P_{\mathrm{r}}^{\mathrm{f,d}} &= \lim_{T\to\infty} \frac{1}{2T} \int_{-T}^{T} \sum_{m,\kappa,n} E[f(m,\kappa,n)^2]dt\,, \\ P_{\mathrm{r}}^{\mathrm{f,c}} &= \lim_{T\to\infty} \frac{1}{2T} \int_{-T}^{T} 2 \sum_{\substack{m,\kappa,n,n' \\ n>n'}} E[f(m,\kappa,n)f(m,\kappa,n')]dt, \end{aligned} \tag{54}$$

where "d" stands for "direct" and "c" for cross-terms. The power $P_{\mathrm{r}}^{\mathrm{f,d}}$ is exactly $P_{\mathrm{r}}^{\mathrm{s}}$ (42) as provided in Section III.B. The complete derivation of $P_{\mathrm{r}}^{\mathrm{f,c}}$ is conducted in Appendix B and final expression is given in (93). Therefore, $P_{\mathrm{r}}^{\mathrm{f}}$ is expressed as

$$\begin{aligned} P_{\mathrm{r}}^{\mathrm{f}} &= P_{\mathrm{r}}^{\mathrm{s}} + P_{\mathrm{r}}^{\mathrm{f,c}}, \\ P_{\mathrm{r}}^{\mathrm{f,c}} &= \sum_{\substack{m,n,n' \\ n'>n}} \wp_m^{n,n'}\,, \end{aligned}$$

$$\begin{aligned} &\wp_m^{n,n'} \\ &= A_m^n A_m^{n'} \mathrm{PRF}_m \left| M_{\Delta\tau_m^{n,n'}}^{\mathrm{PB}}\left(\Delta f_{D,m}^{n,n'}\right)\right| \mathrm{sinc}\left(\pi \Delta f_{D,m}^{n,n'} T_0\right) \\ &\cos\left(\pi \Delta f_{D,m}^{n,n'}(T_0 + 2\tau_m^n) - \phi\left(M_{\Delta\tau_m^{n,n'}}^{\mathrm{PB}}\left(\Delta f_{D,m}^{n,n'}\right)\right)\right. \\ &\left. + \Delta\theta_m^{n,n'}\right), \end{aligned} \tag{55}$$

where $\Delta\tau_m^{n,n'}$, $\Delta f_{D,m}^{n,n'}$ and $\Delta\theta_m^{n,n'}$ are the difference in delay, Doppler frequency and phase between echoes n and n' of beacon m, provided in equations (83) and (85), respectively. The expression of $M_{\Delta\tau_{\mathrm{m}}^{\mathrm{n,n'}}}^{PB}\left(\Delta f_{D,m}^{n,n'}\right)$ is given by

$$\begin{aligned} M_{\Delta\tau_{\mathrm{m}}^{\mathrm{n,n'}}}^{PB}\left(\Delta f_{D,m}^{n,n'}\right) &= M_{\Delta\tau_{\mathrm{m}}^{\mathrm{n,n'}}}\left(\Delta f_{D,m}^{n,n'}\right) * \\ &\mathrm{FT}\left(b_m(u+\tau_m^n-\tau_m^0)\right)\Big|_{f=\Delta f_{D,m}^{n,n'}}, \end{aligned} \tag{56}$$

where $M_{\Delta\tau}(f)$ is the Fourier Transform (FT) of the product of two composite pulses delayed by $\Delta\tau$. The final expression of $M_{\Delta\tau}(f)$ is given by (without proof)

$$\begin{aligned} M_{\Delta\tau}(f) = \; & 2\sqrt{\frac{\pi}{\alpha}} e^{-\pi^2 f^2/\alpha} e^{-\alpha\frac{\Delta_t^2}{4}} e^{-j\pi f(\Delta\tau+\Delta t)}\,. \\ & \left(\cos(\pi f \Delta t) + e^{-\alpha\frac{\Delta t^2}{4}} \mathrm{ch}\left(\frac{\alpha\Delta t\Delta\tau}{2}\right)\right). \end{aligned} \tag{57}$$

Finally, $\phi(M_{\Delta\tau}^{PB}(\Delta f))$ in (55) is the argument of the complex number $M_{\Delta\tau}^{\mathrm{PB}}(\Delta f)$. Note that formula (55) is validated by simulations in Section V.B.

C. Pulse Independency Discussion and Impact on $\mathrm{pw}_m^{\mathrm{eq,n}}$ and $\mathrm{PW}_m^{\mathrm{eq,n}}$

Under the fixed environment assumption, the cross terms $P_{\mathrm{r}}^{\mathrm{f,c}}$ in the average received power $P_{\mathrm{r}}^{\mathrm{f}}$ (55) are not zero and thus the PIC as presented in Section II.B is not fulfilled, since the power of the sum of pulses is not equal to the sum of the individual pulse powers, unless $P_{\mathrm{r}}^{\mathrm{f,c}}$ is negligible with respect to $P_{\mathrm{r}}^{\mathrm{f}}$. Consequently, if $P_{\mathrm{r}}^{\mathrm{f,c}}$ is not negligible with respect to $P_{\mathrm{r}}^{\mathrm{f}}$, the blanker independency as presented in Section II.B does not apply.

If blanker independency does not apply, then it is not possible to express $I_{\mathrm{bdc},m}$ as the reunion of the blanked intervals generated by the individual pulses $I_{\mathrm{bdc},m}^n$ as it was expressed in (37). Indeed, without blanker independency, the sum of the complex envelopes must first be performed, and then $I_{\mathrm{bdc},m}$ must be retrieved by numerical simulation, comparing the envelope of the pulses sum to the blanking threshold $\mathrm{T_H}$ at each instant. The consequences of $I_{\mathrm{bdc},m}$ being numerically obtained for $\mathrm{pw}_m^{\mathrm{eq}}$ and $\mathrm{PW}_m^{\mathrm{eq}}$ are presented next.

First, for $\mathrm{pw}_m^{\mathrm{eq,n}}$, the closed-form formula found for the statistical assumption (41) still holds. However, if $I_{\mathrm{bdc},m}$ does not have a mathematical expression, a numerical simulation must be performed to find the final value of $\mathrm{pw}_m^{\mathrm{eq}}$.

Second, for $\mathrm{PW}_m^{\mathrm{eq}}$, a closed-form formula under the fixed environment assumption which differs from the statistical one (42), is retrieved by identification from (19) and from the expression of the average post blanker received power (55) as

$$\begin{aligned} P_{\mathrm{r}}^{\mathrm{f}} &= \sum_{m=1}^{M} \left(P_{\mathrm{r},m}^{\mathrm{s}} + P_{\mathrm{r},m}^{\mathrm{f,c}}\right), \\ P_{\mathrm{r},m}^{\mathrm{s}} + P_{\mathrm{r},m}^{\mathrm{f,c}} &= \mathrm{PEP}_m^0 \mathrm{PW}_m^{\mathrm{eq}} \mathrm{PRF}_m, \\ \mathrm{PW}_m^{\mathrm{eq}} &= \sum_{n} \frac{\mathrm{PEP}_m^n}{\mathrm{PEP}_m^0} \mathrm{PW}_m^{\mathrm{eq},n} + \sum_{\substack{n,n' \\ n'>n}} \frac{\wp_m^{n,n'}}{\mathrm{PEP}_m^0}. \end{aligned} \tag{58}$$

The closed-form is thus composed of two terms, $\mathrm{PW}_m^{\mathrm{eq},n}$ provided in (50) and $\wp_m^{n,n'}$ given in (55), which both depend on the blanked interval $I_{\mathrm{bdc},m}$: $\mathrm{PW}_m^{\mathrm{eq},n}$ depends on $\mathrm{l}_{\mathrm{d},m}^q$ and $\mathrm{r}_{\mathrm{d},m}^q$ and $\wp_m^{n,n'}$ depends on $b_m(t)$. Therefore, as for $\mathrm{pw}_m^{\mathrm{eq}}$, and additional simulation step must be performed in order to obtain the final value of $\mathrm{PW}_m^{\mathrm{eq}}$ in the case where the PIC is not fulfilled.

D. Definition of Pulse Independency Zones

Since numerical simulations are required where $P_{\mathrm{r}}^{\mathrm{f,c}}$ is not negligible with respect to P_{r}^{s}, zones where $P_{\mathrm{r}}^{\mathrm{f,c}}$ can be neglected (and only a numerical evaluation of the closed-formula is required to obtain $\mathrm{pw}_m^{\mathrm{eq,n}}$ and $\mathrm{PW}_m^{\mathrm{eq}}$), should be defined. In

particular, three pulse independency zones where pulse independencies are evaluated, are defined.

Zone 1: $P_{\mathrm{r}}^{\mathrm{f,c}}$ is negligible with respect to P_{r}^{s} and thus PIC is fulfilled. In that case, $\mathrm{pw}_m^{\mathrm{eq}}$ (41) and PW_m^{eq} (50) of the statistical model can be used, even under the environment fixed assumption.

Zone 2: $P_{\mathrm{r}}^{\mathrm{f,c}}$ is not negligible with respect to P_{r}^{s} but the addition of $P_{\mathrm{r}}^{\mathrm{f,c}}$ and P_{r}^{s} is equal to the power of a resulting a composite pulse with complex amplitude calculated from the sum of the complex amplitudes of the inspected composite pulse. Therefore, $\mathrm{pw}_m^{\mathrm{eq}}$ (41) and PW_m^{eq} (50) of the statistical model can still be used in that zone.

Zone 3: $P_{\mathrm{r}}^{\mathrm{f,c}}$ is neither negligible with respect to P_{r}^{s} nor an equivalent composite pulse, with amplitude equal to the complex amplitude sum of the individual pulses, exists. In that case, $\mathrm{pw}_m^{\mathrm{eq}}$ (41) and $\mathrm{PW}_m^{\mathrm{eq}}$ under the fixed environment must be used (58) and thus numerical simulations must be performed to obtain their final values.

To simplify the mathematical definition of the three zones, the notation of $P_{\mathrm{r,m}}^{s}$ from (42) is updated into

$$\begin{aligned} P_{\mathrm{r,m}}^{s} &= \sum_{n} u_m^n, \\ u_m^n &= \mathrm{PEP}_m^n \mathrm{PW}_m^{\mathrm{eq},n} \mathrm{PRF}_m. \end{aligned} \tag{59}$$

Zones are always defined by fixing a reference scatterer n_0 in the set of the N_m scatterers in the RLOS of beacon m. Once the reference scatterer is set, zones are determined by investigating the average received power as if only two echoes (n_0, n) were received (average pairwise received power), where n goes through $[\![1, N_m - 1]\!]$ since $n \neq n_0$. Note that this restriction to only two echoes is made to facilitate the zones mathematical definitions.

The average pairwise received power under the fixed environment assumptions $P_{\mathrm{r}}^{\mathrm{f}}$ when two echoes (n_0, n) are received using (59) notation is simply expressed as

$$P_{\mathrm{r}}^{\mathrm{f}} = P_{\mathrm{r}}^{\mathrm{s}} + P_{\mathrm{r}}^{\mathrm{f,c}} = u_m^{n_0} + u_m^n + \wp_m^{n_0,n}. \tag{60}$$

Moreover, a new quantity, $u_m^{n_0 \oplus n}$, is defined as the power of a composite pulse which complex amplitude is the sum of the complex amplitudes of pulses n_0 and n as

$$u_m^{n_0 \oplus n} = \frac{\left(A_m^{n_0} + A_m^{n}\right)^2}{2} \mathrm{PW}_m^{\mathrm{eq},n_0 \oplus n} \mathrm{PRF}_m, \tag{61}$$

where $\mathrm{PW}_m^{\mathrm{eq},n \oplus n'}$ is the equivalent pulse width of the resulting equivalent gaussian pulse.

Finally, from (60) and (61), two conditions $\left(\mathrm{C}_1^{n_0,n}\right)$ and $\left(\mathrm{C}_2^{n_0,n}\right)$ are used to define the zones,

$$\begin{aligned} &\left(\mathrm{C}_1^{n_0,n}\right) \quad \left|\frac{\wp_m^{n_0,n}}{u_m^{n_0} + u_m^{n}}\right| < \epsilon_1 \text{ and} \\ &\left(\mathrm{C}_2^{n_0,n}\right) \quad \left|\frac{u_m^{n_0 \oplus n}}{u_m^{n_0} + u_m^{n} + \wp_m^{n_0,n}}\right| > 1 - \epsilon_2, \end{aligned} \tag{62}$$

where ϵ_1 and ϵ_2 are the threshold fixed by the user representing the tolerance to the condition.

Therefore, by applying the literal definition of the zones and considering the two specified conditions, the three zones are mathematically defined as follows,

$$\begin{aligned} Z_{1,m}^{n_0} &:= \left\{n \in [\![0, N_m - 1]\!] \middle| \left(\mathrm{C}_1^{n_0,n}\right)\right\}, \\ Z_{2,m}^{n_0} &:= \left\{n \in [\![0, N_m - 1]\!] \middle| \neg\left(\mathrm{C}_1^{n_0,n}\right) \bigcap \left(\mathrm{C}_2^{n_0,n}\right)\right\}, \\ Z_{3,m}^{n_0} &:= \left\{n \in [\![0, N_m - 1]\!] \middle| \neg\left(\mathrm{C}_1^{n_0,n}\right) \bigcap \neg\left(\mathrm{C}_2^{n_0,n}\right)\right\} \end{aligned} \tag{63}$$

where $\neg(X)$ means that condition X is not fulfilled. Note that a graphical illustration of the pulse independency zones is provided in section V.C, for a simple DME/aircraft scene.

E. Comparison Between the Statistical and the Fixed Environment Models

The statistical and the fixed environment models are compared in terms of strength, weakness, applicable scope and performance disparities.

Strength: The strength of the statistical model is that closed-formulas of $\mathrm{pw}_m^{\mathrm{eq}}$ and $\mathrm{PW}_m^{\mathrm{eq}}$ have been obtained, thanks to the statistical averaging of all possible carrier phases generated by the environment, θ_{e} as provided in (30). Therefore, Therefore, the model is simple and low complex to apply once the propagation channel model parameters have been obtained.

On the contrary, the fixed environment model does not statistically average all the possible outcomes for θ_{e} but it is rather able to provide the C/N_0 degradation for any DME/TACAN RFI environment and for small parts of aircraft trajectories during which θ_{e} can be considered fixed and equal to a given initial value (no modification of the canal environment), as provided in (51). Therefore, the strength of the fixed environment model is its capacity to represent the outcome of any realization of the carrier phase θ_{e} (any possible initial value).

Weakness: For the statistical model, for some DME/TACAN RFI environments, although the model presents the average case, some (or even all) individual realizations (different θ_{e} values) may not be equal to the statistical average case; and thus, the statistical average value may not cover the impact of all the realizations.

For the fixed environment model, in some pulse independency zones, which must first be identified as defined in (63), the closed-form formulas of $\mathrm{pw}_m^{\mathrm{eq}}$ and $\mathrm{PW}_m^{\mathrm{eq}}$ obtained under the statistical model are not applicable and an additional

numerical simulation is required. Therefore, the complexity of the model may be too high to be applied in some RFI environments where the number of scatterers is large.

Applicable scope: The statistical model is designed to be applicable for safety-of-life standardization purposes. Indeed, a worst but probable (the worst average) case must be analyzed to ensure that minimum requirements are met [22]. The worst average case scenario is determined by searching for the worst geographical point (in terms of C/N_0 degradation and operational constraints), setting the DME/TACAN PRF at its maximum (worst) possible value, and by calculating the average C/N_0 degradation.

The fixed environment model applies, on one hand, to specific DME/TACAN RFI environment with a moderate number of scatterers and, on the other hand, to investigate the C/N_0 degradation deviation of one DME/TACAN RFI signal realization with respect to the statistical average C/N_0 degradation provided by statistical model based on the pulse independency zones analysis (zones where pulse independency condition is not fulfilled in the fixed environment model whereas in the statistical model, pulse independency condition was always demonstrated to be satisfied by assuming that all received DME/TACAN RFI signals θ_e were uniformly distributed).

Performance disparity: Up to now, the fixed environment model has only been used to identify the pulse independency zones creating a C/N_0 degradation deviation of one DME/TACAN RFI realization with respect to the average C/N_0 degradation provided by statistical model (see Section V.C).. Furthermore, numerical disparity between the statistical model proposed in this article and the MP-free $C/N0$ degradation model are provided for two low-altitude hot-spots, JALTO (Philadelphia) and TIXAK (Frankfurt) in the second part of this two-part manuscript [16]. It is shown that the range of the additional $C/N0$ degradation generated by the DME/TACAN MP RFI signal ranges from 0.1 to 0.3 dB [16].

V. SIMULATIONS

In this section, the average received power formula under the statistical (36) and the fixed environment (55) assumption are validated by means of Monte-Carlo simulations. The validation is done by generating time series realizations of the DME/TACAN received RFI signal in presence of MP in Sections V.B and V.C, respectively. Furthermore, a graphical analysis of the Pulse Independency Zones (as developed in Section IV.D is provided) in Section V.D.

A. Preliminary Discussion

In this section, the mathematical models of the average received power formula under the statistical (36) and the fixed environment (55) assumptions are validated. These models are based on the use of the MP parameters as inputs and accept any realistic set of values: any positive number of received MP N_m, and for each MP, any positive PEP, PEP_m^n, delay, τ_m^n, Doppler frequency, $f_{D,m}^n$ and additional phase θ_m^n. Therefore, to validate the models, it is only necessary to ensure that, for different sets of realistic MP parameter values, the average received power predicted by the proposed mathematical models (36) and (55) matches with the average received power obtained through simulations. Therefore, different configurations of MP parameters are tested through Monte-Carlo simulations to validate both models.

Note that in Part II of this companion paper, a propagation channel model is developed to predict the set of MP parameters generated by a given scene [16]; in Part II propagation channel model verification, it would thus be ideal to compare the theoretical prediction with MP parameters extracted from measurements. For a discussion on the measurement acquisition and MP parameters extraction, the reader is referred to [16].

B. Validation of the Average Received Power Formula Under the Statistical Assumption

Formula of the post-blanker average received power (42) using the expressions of $\mathrm{PW}_m^{\mathrm{eq},n}$ provided in (50) and $\mathrm{pw}_m^{\mathrm{eq}}$ given in (41) is validated by means of Monte-Carlo simulations.

The objective of the Monte-Carlo simulations is to demonstrate that for each pair (τ_1, τ_2), the maximum ratio considering all triplets of PEPs $(\mathrm{PEP}^0, \mathrm{PEP}^1, \mathrm{PEP}^2)$, $\mathrm{V}^{\mathrm{s}}(\tau_1, \tau_2)$ (in dB), between the average received powers computed by the Monte-Carlo simulation, $P_{\mathrm{r,MC}}^{s}(\tau_1, \tau_2)$, with respect to the received power formula $P_{\mathrm{r}}^{s}(\tau_1, \tau_2)$ provided in (42) and (50), is below 0.1 dB, i.e.,

$$\mathrm{V}^{\mathrm{s}}(\tau_1, \tau_2) = \max_{\begin{pmatrix}\mathrm{PEP}^0\\ \mathrm{PEP}^1\\ \mathrm{PEP}^2\end{pmatrix}} \left(10 \log_{10}\left(\frac{P_{\mathrm{r,MC}}^{s}(\tau_1, \tau_2)}{P_{\mathrm{r}}^{s}(\tau_1, \tau_2)}\right)\right) \leq 0.1 \text{ dB}. \quad (64)$$

The deterministic and random parameters of the Monte-Carlo simulation are summarized in the first column of Table I. A single DME beacon, three pairs of pulses, with two being MP ($M = 1$, $N_m = 2$ and $N_m^{\mathrm{p}} = 5$) with PEPs ranging from -118 and -121 dBW and one pulse emission ($\mathrm{K}_m = 1$) are considered with emission time $t_1^1 = 0$, and thus the sub-index m and the upper-index κ are discarded from the notation of τ, f and θ. The Doppler frequency of each pair is assumed to be equal to 0. Furthermore, since $M = \mathrm{K} = 1$, the emitted pair can be assumed to be received at $\tau^0 = 0$.

The delay of the two MP varies from 0 to 22 μs and for each pair (τ^1, τ^2) and thus, for the verification of the post-blanker average received power under the statistical assumption, a matrix where each line represents one value of the delay of the MP 1 τ^1, and each column represents one value of the delay of the MP 2 τ^2 is provided.

Table I
Parameters definition for the Monte-Carlo simulations under the statistical and fixed environment assumptions. The sub-index m is discarded since only one beacon ($M = 1$) is considered.

		Statistical Section V.A	Fixed Environment Section V.B
Deterministic Parameters	N_{MC}	10 000	10 000
	N_m	2	1
	T_0 (ms)	-	20
	K	1	54
	PEP^n (dBW)	$\in$ [-121,-118] Step = 1	$\in$ [-130,-121] Step = 3
	τ^1 (μs)	$\in$ [0,22] Step = 0.4	$\in$ [0,22] Step = 1
	τ^2 (μs)	$\in$ [0,22] Step = 0.4	-
	θ_{e}^n	-	$\in [0,2\pi)^2$
	f_{D}^n	0	0 $\forall(\kappa,n)$
	t_m^κ	0	-
Random Parameters	X	$X^{\mathrm{s}} = \begin{pmatrix}\theta_0\\ \theta_{\mathrm{e}}^0\\ \theta_{\mathrm{e}}^1\\ \theta_{\mathrm{e}}^2\end{pmatrix}$	$X^{\mathrm{fe}} = \begin{pmatrix}t^1\\ \vdots\\ t^{\mathrm{K}}\\ \theta_0^1\\ \vdots\\ \theta_0^{\mathrm{K}}\end{pmatrix}$

The methodology to obtain $\mathrm{V}^{\mathrm{s}}(\tau_1,\tau_2)$ is as follows.

First, one triplet $(\mathrm{PEP}^0,\mathrm{PEP}^1,\mathrm{PEP}^2) \in [-118,-121]^3$ is selected and N_{MC} draws of the random vector X^{s} are realized. X^{s} contains all the random parameters which allow to obtain one realization of the random signal $r(t)$ expressed in (29).

Second, for one draw X_i^{s}, $i \in [1, N_{\mathrm{MC}}]$ of X^{s}, and using the deterministic parameters of the simulation, one complex representation $r_i^{\mathrm{s,cr}}(t,\tau^1,\tau^2)$ of the pre-blanker RFI signal is determined as

$$\begin{aligned} r_i^{\mathrm{cr}}(t,\tau^1,\tau^2) &= \sum_{n=0}^{N_m} r_{i,n}^{\mathrm{cr}}(t,\tau^n), \\ r_{i,n}^{\mathrm{cr}}(t,\tau^n) &= A^n\big(s_{\mathrm{bb}}(t-\tau^n)\big)e^{j\left(2\pi f+\theta_{0,i}+\theta_{\mathrm{D}}^n+\theta_{\mathrm{e},i}^n\right)}, \\ A^n &= \sqrt{2\mathrm{PEP}^n} \end{aligned} \tag{65}$$

where $r_{i,n}^{\mathrm{cr}}$ represents the complex representation of MP n of draw i. Note that the carrier frequency f chosen in this study does not matter since each direct and MP pairs are assumed to come from the same beacon and thus have the same carrier frequency that is to be removed when taking the modulus of $r_i^{\mathrm{cr}}(t,\tau^1,\tau^2)$.

Third, the complex envelope r_i^{ce} of r_i^{cr} is derived by taking the squared modulus of r_i^{cr}, i.e., $r_i^{\mathrm{ce}}(t,\tau^1,\tau^2) = |r_i^{\mathrm{cr}}(t,\tau^1,\tau^2)|^2$.

Fourth, from $r_i^{\mathrm{ce}}(t,\tau^1,\tau^2)$, the post-blanker complex envelope $r_{i,\mathrm{b}}^{\mathrm{ce}}(t,\tau^1,\tau^2)$ is obtained by deriving the blanked intervals generated by the direct and the two MP pairs according to (41).

Fifth, from the temporal expression of $r_{i,\mathrm{b}}^{\mathrm{ce}}(t,\tau^1,\tau^2)$, the time series of $r_{i,\mathrm{b}}^{\mathrm{ce}}(t,\tau^1,\tau^2)$ are generated in MATLAB, with a sampling frequency of 100 MHz. Note that in $r_{i,\mathrm{b}}^{\mathrm{ce}}$ the blanked intervals are derived under the BIA, i.e., the blanked intervals generated by each pair have been derived as if the only received pair was pair n.

Sixth, the simulated received power $P_{\mathrm{r,MC},i}^{\mathrm{s}}(\tau_1,\tau_2)$, $i \in [1, N_{\mathrm{MC}}]$, is obtained by integrating the generated time series of $r_{i,\mathrm{b}}^{\mathrm{ce}}(t,\tau^1,\tau^2)$ in MATLAB by means of the classical trapeze integration method. Once all the $P_{\mathrm{r,MC},i}^{\mathrm{s}}$ have been determined, the value of $P_{\mathrm{r,MC}}^{\mathrm{s}}(\tau_1,\tau_2)$ is obtained by averaging all the $P_{\mathrm{r,MC},i}^{\mathrm{s}}(\tau_1,\tau_2)$, i.e.,

$$\begin{aligned} P_{\mathrm{r,MC}}^{\mathrm{s}}(\tau_1,\tau_2) &= \frac{1}{N_{\mathrm{MC}}}\sum_{i=1}^{N_{\mathrm{MC}}} P_{\mathrm{r,MC},i}^{\mathrm{s}}(\tau_1,\tau_2), \\ P_{\mathrm{r,MC},i}^{\mathrm{s}}(\tau_1,\tau_2) &= \int_{-\infty}^{\infty} r_{i,\mathrm{b}}^{\mathrm{ce}}(t,\tau_1,\tau_2)dt \end{aligned} \tag{66}$$

where the integral in (66) is only obtained numerically.

Finally, the value of $P_{\mathrm{r,MC}}^{\mathrm{s}}(\tau_1,\tau_2)$ obtained by simulation is compared to the theoretical value of $P_{\mathrm{r}}^{\mathrm{s}}(\tau_1,\tau_2)$ determined from (42) and (50) by calculating the ratio between $P_{\mathrm{r,MC}}^{\mathrm{s}}(\tau_1,\tau_2)$ and $P_{\mathrm{r}}^{\mathrm{s}}(\tau_1,\tau_2)$. The process is repeated for each possible triplet $(\mathrm{PEP}^0,\mathrm{PEP}^1,\mathrm{PEP}^2)$ and the value of $\mathrm{V}^{\mathrm{s}}(\tau_1,\tau_2)$ is determined by taking the maximum of all the obtained ratios. The final validation matrix composed of all $\mathrm{V}^{\mathrm{s}}(\tau_1,\tau_2)$ is provided in Fig. 8.

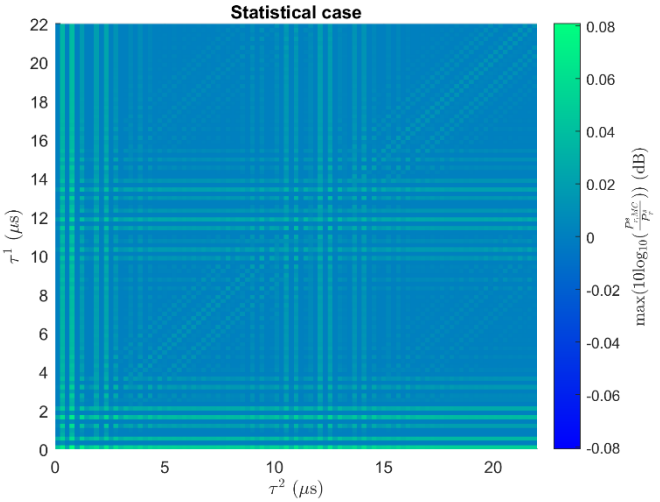

Fig. 8. Results of the Monte-Carlo simulations for the average received power P_r^{s} under the statistical assumption.

Fig. 8 shows that the ratio between $P_{\mathrm{r}}^{\mathrm{s}}$ (42) and $P_{\mathrm{r,MC}}^{\mathrm{s}}$ never exceed 0.08 dB and thus the formulas of the average received

power under the statistical assumption P_r^s (42) and (50) are validated.

C. Validation of the Average Received Power Formula Under the Fixed Environment Assumption

The formula of the post-blanker average received power (55) is validated by means of Monte-Carlo simulations.

The objective of the Monte-Carlo simulations is to demonstrate that, for each delay τ^1, the maximum ratio considering all pairs of PEPs $(\text{PEP}^0, \text{PEP}^1)$, $\text{V}^{\text{fe}}(\tau^1)$ (in dB), between an average received power computed by the Monte-Carlo simulation, $P_{\text{r,MC}}^{\text{f}}(\tau^1)$ with respect to the received power formula $P_{\text{r}}^{\text{f}}(\tau^1)$ provided in (55) is below 0.1 dB, i.e.,

$$\text{V}^{\text{fe}}(\tau^1) = \max_{\binom{\text{PEP}^0}{\text{PEP}^1}} \left(10 \log_{10} \left(\frac{P_{\text{r,MC}}^{\text{f}}(\tau^1)}{P_{\text{r}}^{\text{f}}(\tau^1)} \right) \right) \leq 0.1 \text{ dB}. \quad (67)$$

The deterministic and random parameters of the Monte-Carlo simulation are provided in the second column of Table I. In comparison with the statistical case (see Section V.A), a single DME beacon, one LOS and one MP ($M = 1$, $N_m = 1$ and $N_m^{\text{p}} = 3$) with PEP = -121 dBW PEPs ranging from -121 and -130 dBW and 54 pulse pair emissions ($\text{K}_m = 54$), since the time of observation is $T_0 = 20$ ms, are considered. T_0 is set to 20 ms to simulate a short time when the channel time dependent properties can be assumed to be unchanged. Therefore, for this simulation, θ_{e}^0 and θ_{e}^1 are just two constants derived from two draws of an uniform law on $[0,2\pi)$.

The additional delay τ^1 of the unique MP spans from 0 to 22 µs with a 1 µs step and thus, for the verification of the post-blanker average received power under the FEA, V^{fe} is a line vector of size the number of possible values of τ^1.

The methodology to obtain $\text{V}^{\text{fe}}(\tau^1)$ is exactly the same as for the statistical case, except for the blanking step since all the received pulses are assumed to have a PEP below the blanking threshold: for each draw i of X^{fe}, X_i^{fe}, the time series of the complex envelope of a realization of the received signal as provided in (52) is generated in MATLAB. Then, $P_{\text{r,MC}}^{\text{f}}(\tau^1)$ is obtained by averaging all the $P_{\text{r,MC},i}^{\text{f}}(\tau^1)$ determined by the numerical trapeze integration of the complex envelopes. The process is repeated for each possible pair $(\text{PEP}^0, \text{PEP}^1)$ and the value of $\text{V}^{\text{s}}(\tau_1)$ is determined by taking the maximum of all the obtained ratios.

Fig. 9 provides (a) the validation vector V^{fe} and (b) the outputs of $P_{\text{r,MC}}^{\text{f}}(\tau^1)$ (in straight line) and $P_{\text{r}}^{\text{f}}(\tau^1)$ (in dashed line) in W, for three different pairs $(\text{PEP}^0, \text{PEP}^1)$.

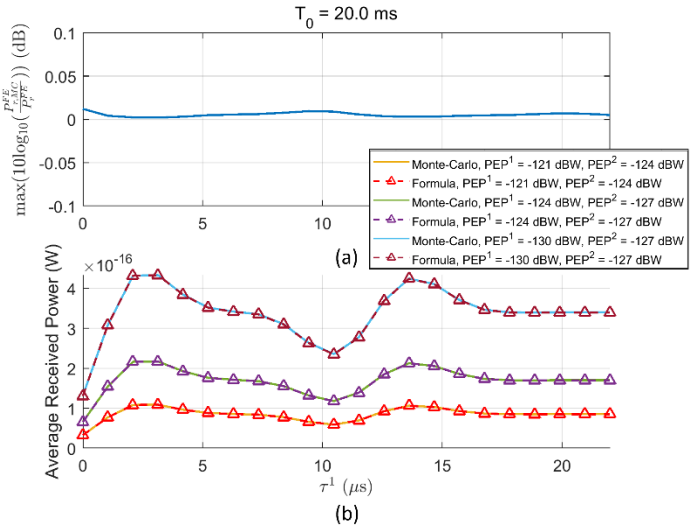

Fig. 9. (a) Results of the validation vector V^{f} for the Monte-Carlo simulations under the fixed environment assumption and (b) outputs of $P_{\text{r,MC}}^{\text{f}}(\tau^1)$ (in straight line) and $P_{\text{r}}^{\text{f}}(\tau^1)$ (in dashed line) in W, for three different pairs $(\text{PEP}^0, \text{PEP}^1)$.

Fig. 9 (a) shows that the ratio between $P_{\text{r,MC}}^{\text{f}}$ and P_{r}^{f} (55) never exceeds 0.05 dB and thus the formula obtained for the average power under the fixed environment assumption P_{r}^{f} (55) is validated.

D. Illustration of Pulse Independency Zones

In this section, four graphical analyses of the pulse independency zones are provided for a single DME beacon/aircraft scene. This scene is representative of the single DME beacon/aircraft scene that can be found at the two low-altitude operational hot-spots JALTO (Philadelphia, US) and TIXAK (Frankfurt, Germany); note that these operational hot-spots scenes are investigated in the second part of this two part manuscript [16]. First, the objective of the simulation is introduced. Second, a description of the scene and the different illustration parameters are given. Third, the methodology to determine the pulse independency zones is introduced. Finally, the four analyses are provided and the results are discussed.

Objective: The objective of this simulation is to provide a graphical illustration of the pulse independency zones, defined in Section IV.D in a representative real-world scenario. The pulse independency zones provide the set of scatterers where, relatively to a reference scatterer, the closed-form formulas of pw_m^{eq} (41) and PW_m^{eq} (50) obtained for the statistical assumption (53) are applicable (Zone 1), are applicable after combining pulses into one composite pulse (Zone 2) or are not directly applicable (Zone 3).

Scene description and parameters definition: The scene is composed of a single DME beacon and an aircraft separated by a distance of 50 km in the horizontal plane. A single beacon/aircraft scene is considered since the contribution to the statistical average received power for the fixed environment assumption of one individual DME/TACAN beacon is

independent from the contribution of the remaining DME/TACAN beacons inside the aircraft RLOS (58) (note that this statement also holds for the statistical assumption case). The aircraft is supposed to be in a real-world approach phase, that is, at 2100 feet above ground, its velocity is set to 115 knots and its glide angle to 5° [26]. The aircraft speed vector direction in the azimuthal plane is set to be either North or East. Note that, since only one beacon is considered, the subindex m is removed from the remaining part of the section.

The set of scatterers generating a MP is all the points on the ground within the RLOS of the DME beacon, defined as a circle around the beacon with a radius of 25 km which is the average value of the RLOS found for JALTO and TIXAK [16]. Therefore, there are as many scatterers as the number of discrete points covered during the full sweep of the RLOS. The PEP of any scatterers within the RLOS is set to -122 dBW and thus the blanker is never triggered.

The beacon carrier frequency f is set to the mode X carrier frequency 1176 MHz and the pulse repetition frequency PRF is set to 2700. The tolerance ϵ_1 and ϵ_2 are set to be equal to ϵ, i.e., $\epsilon = \epsilon_1 = \epsilon_2$ and ϵ can take two different values, 0.01 or 0.05. The difference in additional phase $\Delta\theta^{n_0,n}$ is set to 45°. Note that only one value of $\Delta\theta^{n_0,n}$ is chosen for these analyses since the influence of $\Delta\theta^{n_0,n}$ was found to only have a small impact on the final results.

The value of T_0 is discussed next. A short value T_0 implies a larger zone 3, because the potential full sweep of the phase difference (statistical assumption) is unlikely to happen during that short time; for a given $\Delta f_{\mathrm{D}}^{n_0,n}$, a larger time T_0 allows for a larger phase sweep, $2\pi\Delta f_{\mathrm{D}}^{n_0,n}T_0$. Therefore, zone 3 is expected to shrink and zone 1 is expected to grow as T_0 increases. Therefore, two values of T_0, 20 ms and 1 s, are investigated to illustrate this phenomenon.

Methodology: The methodology for identifying the pulse independency zones of each analyzed reference scatter is as follows.

First, the zone matrix $\mathcal{Z}$ is determined for generic values of $\Delta\tau$ and Δf_D. Matrix $\mathcal{Z}$ is defined as the matrix where each element $\mathcal{Z}_{\Delta\tau,\Delta f_D}$ represents the pulse independency zone (Zone 1,2 or 3) of a scatterer whose additional delay and Doppler frequency with respect to the direct pair is $(\Delta\tau, \Delta f_D)$. The determination of the pulse independency zones is obtained by the derivation $\wp^{n_0,n}$, u^{n_0}, u^n and $u^{n_0\oplus n}$ from $(\Delta\tau, \Delta f_D)$ and the inputs of the simulations using equations (61),(59) and (55). The sets of values of $\Delta\tau$ and Δf_D over which $\mathcal{Z}_{\Delta\tau,\Delta f_D}$ is computed is conservatively chosen to be $[-200,200]$ µs for $\Delta\tau$ (with a step of 0.5 µs) and $[-200,200]$ Hz for Δf_D (with a step of 0.5 Hz) to ensure that every scatterer additional delay and Doppler frequency $\left(\Delta\tau^{n_0,n}, \Delta f_{\mathrm{D}}^{n_0,n}\right)$ in the RLOS lies within that range.

Second, the position of the reference scatterers is chosen. For this illustration, 4 different reference scatterers are defined and situated at the coordinates $(50 \pm 12.5, \pm 12.5)$, respectively.

Third, a full sweep of the RLOS is realized using two parameters $\mathcal{R}$ and ϑ, where $\mathcal{R}$ and ϑ span from $[0, \mathrm{RLOS})$ m and $[0,2\pi)$ radians, with a step of 50 m and 0.01 rad, respectively, which means that, in total, 250 000 scatterers (with respect to each reference scatterer) are investigated. For each scatterer, the pair $\left(\Delta\tau^{n_0,n}, \Delta f_{\mathrm{D}}^{n_0,n}\right)$ is determined and the scatterer is assigned to one zone by looking at the closest pair $(\Delta\tau, \Delta f_D)$ in $\mathcal{Z}$.

Results: Using the presented methodology, the simulations are processed and the illustration results are provided in Fig. 10 and Fig. 11 for $\epsilon = 0.05$ and $\epsilon = 0.01$, respectively. For each illustration, the aircraft velocity azimuth angle is directed either to (a) North or to (b) East. Two different sets of colors are assigned to the 3 pulse independency zones for the two different values of T_0. For $T_0 = 20$ ms, Zones 1, 2 and 3 are respectively displayed in white, blue and red. For $T_0 = 1$ s, Zone 1, 2 and 3 are respectively displayed in white, cyan and orange. The DME beacon, the aircraft and the four reference scatterers are represented by a green dot, a red dot and black squares, respectively. Finally, the RLOS and the aircraft speed vector are shown as a black line and a red arrow.

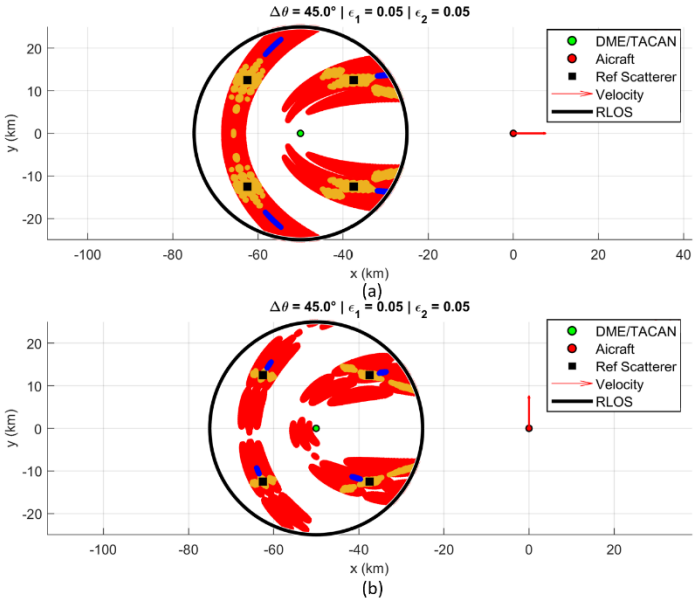

Fig. 10. Graphical illustration of the pulse independency zones for $\epsilon_1 = \epsilon_2 = 0.05$, $T_0 = 20$ ms or 1 s and aircraft velocity (a) North and (b) East.

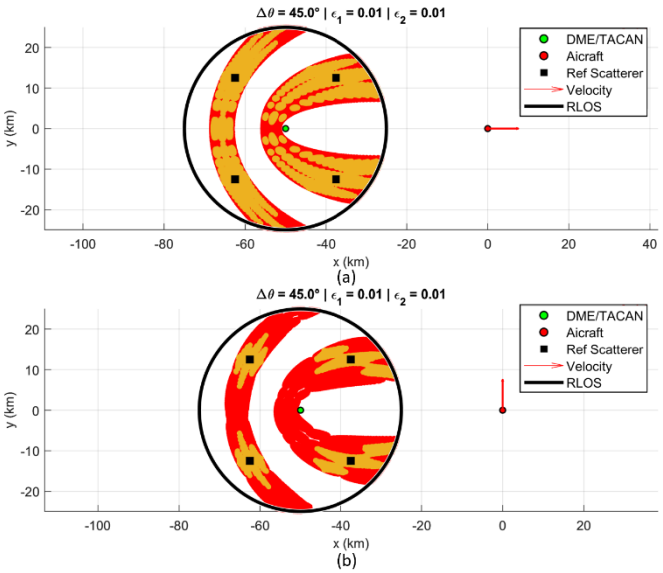

Fig. 11. Graphical illustration of the pulse independency zones for $\epsilon = 0.01$, $T_0 = 20$ ms or 1 s and aircraft velocity (a) North and (b) East.

Three concluding remarks can be made regarding Fig. 10 and Fig. 11:

1. Zone 2 associated with $T_0 = 1$ s (cyan) is not visible in both figures since only scatterers extremely close to the reference scatterers can be combined to create a composite pulse which complex amplitude is the sum of original pulses complex amplitudes. Therefore, zone 2 is too small to be seen in the plot.
2. The decrease of thresholds $\epsilon = \epsilon_1 = \epsilon_2$ implies a smaller tolerance to $\left(\mathrm{C}_1^{n_0,n}\right)$ expressed in (62). Therefore, less scatterer verify $\left(\mathrm{C}_1^{n_0,n}\right)$ and thus zone 3 increases for $\epsilon = 0.01$ with respect to $\epsilon = 0.05$.
3. The increase of T_0 implies a decrease of zones 2 and 3. The reason is that the full sweep of the phase difference is more likely to happen when T_0 increases (as previously explained).

VI. CONCLUSION

In this manuscript (part I), two models of the GNSS signal C/N_0 degradation at the correlator input of the future airborne GNSS DMFC receiver have been introduced to account for the degradation generated by the received DME/TACAN MP RFI signals in addition to the DME/TACAN LOS RFI signals (already provided in [1]). The derivation of the formulas is done by updating the general original MP-free formulas of $\mathrm{pw}_m^{\mathrm{eq}}$ and $\mathrm{PW}_m^{\mathrm{eq}}$ with the presence of multiple DME/TACAN echoed pulses.

The first derived model is the statistical model. In this model, the additional phase generated by the propagation channel environment (atmospheric and weather conditions, composition and temporal properties of the scatterers facades, etc.), θ_{e}, is considered unknown and thus is assumed to follow a uniform distribution. Therefore, this model provides a statistical average of the GNSS signal C/N_0 degradation by averaging all the possible outcomes of θ_{e} in $[0,2\pi)$; as a consequence, while this model may not be able to capture the C/N_0 degradation of one individual carrier phase situation (only the average is provided), it can be used to find the worst but probable average case of the C/N_0 degradation generated by DME/TACAN RFI LOS and MP signals if other parameters, such as the geographical location and the signal PRF are set to their worst values.

Under the statical modelling of θ_{e}, it has been shown that the PIC (power of the sum of multiple pulses is equal to the sum of the individual power generated by each pulse) was fulfilled and thus closed-form formulas of $\mathrm{pw}_m^{\mathrm{eq}}$ and $\mathrm{PW}_m^{\mathrm{eq}}$ were derived. Therefore, the main strength of this model is its low complexity due to the use of $\mathrm{pw}_m^{\mathrm{eq}}$ and $\mathrm{PW}_m^{\mathrm{eq}}$ closed-form formulas, once its inputs are determined by a propagation channel model.

As a conclusion, this model is particularly suitable for safety-of-life standardization when analyzing RFI environment with a very large number of scatters. An example of GNSS signal C/N_0 degradation statistical model application is given in the second part of this two-part manuscript to determine the degradation generated by DME/TACAN RFI LOS and MP signals at two operational hot-spots: JALTO (Philadelphia) and TIXAK (Frankfurt) [16].

The second derived model is the fixed environment model. In this model, θ_{e} is assumed to be constant and equal to his initial value for a short time T_0, where environmental conditions can be assumed constant. The strength of this model is that it can be used to calculate any C/N_0 degradation of any individual carrier phase situation (any initial and constant value of θ_{e}).

Under this modelling of θ_{e}, it has been shown that the PIC was not always perfectly fulfilled and thus closed-form formulas of $\mathrm{pw}_m^{\mathrm{eq}}$ and $\mathrm{PW}_m^{\mathrm{eq}}$ can just provide a loose approximation of the true value (the accuracy of the approximation depending on the observation time). Therefore, pulse independency zones, where the closed-form formulas from the statistical model can be used with a given degree of accuracy have been mathematically defined.

However, when a higher degree of C/N_0 degradation accuracy is demanded, the fixed environment model requires an additional simulation step to be performed outside the PIC. Therefore, the complexity of this model is probably too high to be applied in RFI environments where the number of scatterers is large if high precision is required; if not, its application and result are equivalent to the statistical model. Therefore, for now, the fixed environment model is only used to identify zones creating a C/N_0 degradation deviation (equivalent to a loss of accuracy) of one DME/TACAN RFI realization with respect to the average C/N_0 degradation provided by statistical model.

In this manuscript, the number of MP N_m and the additional delay τ_m^n and amplitude A_m^n of each MP have been assumed to be provided by the air-ground propagation channel developed in Part II of this two part manuscript [16] for both models. As such, they have been assumed to be deterministic in this work (partial reduction of the uncertainty of the MP parameters). The limitations associated with the deterministic modelling of N_m, τ_m^n and A_m^n are that it requires a highly detailed scene to be given as an input of the air-ground propagation channel [16] and to select a final value of A_m^n (all the uncertainty of A_m^n can not be removed by the scene and the propagation channel model); in this work, the statistical mean for A_m^n has been chosen.

Both models have been validated by means of Monte-Carlo simulations, by generating time series realizations of the received DME/TACAN RFI signals. Furthermore, a graphical illustration of the pulse independency zones have been presented for a simple scene composed of a single DME beacon and the aircraft.

Future works include the analysis of the coupling between the ADC/AGC and the blanker, and the exact modelling of SSC in presence of the temporal blanker and the MP.

APPENDIX A
Average Power Derivation – Statistical Assumption

In this appendix, the derivation of the average power of $r(t)$ (29) under the statistical assumption (30) is conducted. In the statistic case, the average power P_{r}^{s} from (35) is given by

$$P_{\mathrm{r}}^{s} = \lim_{T\to\infty} \frac{1}{2T} \int_{-T}^{T} \sum_{m,\kappa,n} E[f(m,\kappa,n)^2] dt\,. \tag{68}$$

where

$$\begin{aligned} E[f(m,\kappa,n)^2] = (A_m^n)^2 E[g(t-t_m^\kappa-\tau_m^n)^2 \cdot \\ b_m(t-t_m^\kappa-\tau_m^0)^2 \cos\big(2\pi\big(f_m+f_{D,m}^n\big)t \\ +\theta_m^{\kappa,n}\big)^2]. \end{aligned} \tag{69}$$

Furthermore, $b_m(t-t_m^\kappa-\tau_m^0)^2 = b_m(t-t_m^\kappa-\tau_m^0)$, $t_m^\kappa \perp \theta_m^{\kappa,n}$ and $\cos^2(x) = \frac{1-\cos(2x)}{2}$. Therefore,

$$\begin{aligned} E[f(m,\kappa,n)^2] = \frac{(A_m^n)^2}{2} E[g(t-t_m^\kappa-\tau_m^n)^2 b_m(t \\ -t_m^\kappa-\tau_m^0)], \end{aligned} \tag{70}$$

since, by the law of total expectation,

$$E\big[\cos\big(4\pi\big(f_m+f_{D,m}^n\big)t+2\theta_m^{\kappa,n}\big)\big] = 0. \tag{71}$$

Furthermore, since $t_m^\kappa \sim U[0,T_0]$

$$\begin{aligned} P_{\mathrm{r}}^{s} = \lim_{T\to\infty} \frac{1}{2T} \int_{-T}^{T} \sum_{m,\kappa,n} \frac{(A_m^n)^2}{2T_0} \int_{0}^{T_0} g(t-t_m^\kappa \\ -\tau_m^n)^2 b_m(t-t_m^\kappa-\tau_m^0) dt_m^\kappa\, dt\,. \end{aligned} \tag{72}$$

Assume $\mathrm{K}_m(T)$ to be the number of received pulse pairs during $[-T,T]$, then, interchanging sums (where now $\kappa \in [\![1, \mathrm{K}_m(t)]\!]$) and integral and using Fubini's theorem,

$$\begin{aligned} P_{\mathrm{r}}^{s} &= \lim_{T\to\infty} \frac{1}{2T} \sum_{m,\kappa,n} \frac{\mathrm{PEP}_m^n}{T_0} \int_{0}^{T_0} I(t_m^\kappa)\, dt_m^\kappa \\ I(t_m^\kappa) &= \int_{-T}^{T} h(t) dt \\ h(t) &= g(t-t_m^\kappa-\tau_m^n)^2 b_m(t-t_m^\kappa-\tau_m^0) \end{aligned} \tag{73}$$

Therefore, there is no term inside the sum which depends on κ since dependency on t_m^κ is removed by the integral. This yields,

$$\begin{aligned} P_{\mathrm{r}}^{s} &= \lim_{T\to\infty} \frac{1}{2T} \sum_{m,n} \frac{K_m(T)\mathrm{PEP}_m^n}{T_0} \int_{0}^{T_0} I(t_m^\kappa)\, dt_m^\kappa \\ P_{\mathrm{r}}^{s} &= \sum_{m,n} \lim_{T\to\infty} \Big(P_{\mathrm{r}}^{s,1}(T) \cdot P_{\mathrm{r}}^{s,2}(T)\Big), \end{aligned} \tag{74}$$

where

$$\begin{aligned} P_{\mathrm{r}}^{s,1}(T) &= \frac{K_m(T)}{2T}, \\ P_{\mathrm{r}}^{s,2}(T) &= \frac{\mathrm{PEP}_m^n}{T_0} \int_{0}^{T_0} I(t_m^\kappa)\, dt_m^\kappa. \end{aligned} \tag{75}$$

Assuming that both limits of $P_{\mathrm{r}}^{s,1}(T)$ and $P_{\mathrm{r}}^{s,2}(T)$ are finites (which will be shown later in the derivation), the limit can be linearized into

$$P_{\mathrm{r}}^{s} = \sum_{m,n} \lim_{T\to\infty} \Big(P_{\mathrm{r}}^{s,1}(T)\Big) \cdot \lim_{T\to\infty} \Big(P_{\mathrm{r}}^{s,2}(T)\Big), \tag{76}$$

where

$$\begin{aligned} \lim_{T\to\infty} \Big(P_{\mathrm{r}}^{s,1}(T)\Big) &= \lim_{T\to\infty} \left(\frac{K_m(T)}{2T}\right) \\ &= \mathrm{PRF_m} \end{aligned} \tag{77}$$

as PRF is defined as an average pulse repetition frequency and

$$\begin{aligned}\lim_{T\to\infty}\left(P_{\mathrm{r}}^{s,2}(T)\right) &= \lim_{T\to\infty}\left(\frac{\mathrm{PEP}_m^n}{T_0}\int_0^{T_0} I(t_m^\kappa)\,dt_m^\kappa\right)\\ &= \frac{\mathrm{PEP}_m^n}{T_0}\int_0^{T_0}\lim_{T\to\infty}\int_{-T}^{T} h(t)dtdt_m^\kappa \qquad (78)\\ &= \frac{\mathrm{PEP}_m^n}{T_0}\int_0^{T_0}\int_{-\infty}^{\infty} h(t)dtdt_m^\kappa.\end{aligned}$$

Furthermore,

$$\begin{aligned}\int_{-\infty}^{\infty} h(t)dt &= \int_{-\infty}^{\infty} g(t-t_m^\kappa-\tau_m^n)^2 b_m(t-t_m^\kappa-\tau_m^0)dt\\ &= \int_{-\infty}^{\infty} e^{-\alpha(u-\tau_m^n)^2} b_m(u-\tau_m^0)du\end{aligned} \qquad (79)$$

which does not depend on κ. Therefore, from (76), the final expression of $P_{\mathrm{r}}^{\mathrm{s}}$ is given by

$$\begin{aligned}P_{\mathrm{r}}^{\mathrm{s}} &= \sum_{m,n}\frac{\mathrm{PRF_m PEP}_m^n}{T_0}\int_0^{T_0}\int_{-\infty}^{\infty} h(t)dt\,dt_m^\kappa\\ &= \sum_{m,n}\mathrm{PRF_m PEP}_m^n\int_{-\infty}^{\infty} e^{-\alpha(u-\tau_m^n)^2} b_m(u-\tau_m^0)du\,.\end{aligned} \qquad (80)$$

APPENDIX B
Average Power Derivation – Fixed Environment Assumption

In this appendix, the derivation of the average power of $r(t)$ (52) under the fixed environment assumption (53) is conducted. In the fixed environment case, the average received power $P_{\mathrm{r}}^{\mathrm{f}}$ (54) is given by

$$\begin{aligned}P_{\mathrm{r}}^{\mathrm{f}} &= P_{\mathrm{r}}^{\mathrm{s}} + P_{\mathrm{r}}^{\mathrm{f,c}},\\ P_{\mathrm{r}}^{\mathrm{f,c}} &= \lim_{T\to\infty}\frac{1}{2T}\int_{-T}^{T} 2\sum_{\substack{m,\kappa,n,n'\\ n>n'}} E[f(m,\kappa,n)f(m,\kappa,n')]dt,\end{aligned} \qquad (81)$$

where $P_{\mathrm{r}}^{\mathrm{s}}$ is provided in (80). Let $E_f^{n,n'}$ be $E[f(m,\kappa,n)f(m,\kappa,n')]$ then, since $t_m^\kappa \perp \theta_m^{\kappa,n}$,

$$\begin{aligned}E_f^{n,n'} &= A_m^n A_m^{n'}\cdot\\ &E\left[m_{\Delta\tau_m^{n,n'}}(t-t_m^\kappa-\tau_m^n)b_m(t-t_m^\kappa-\tau_m^0)^2\right]\cdot\\ &E[\cos\left(\left(2\pi\left(f_m+f_{D,m}^n\right)t+\theta_m^{\kappa,n}\right)\right)\cdot\\ &\cos\left(\left(2\pi\left(f_m+f_{D,m}^{n'}\right)t+\theta_m^{\kappa,n'}\right)\right)],\end{aligned} \qquad (82)$$

where $m_{\Delta\tau}(t)$ is the product of two pulse pairs delayed by $\Delta\tau$ and $\Delta\tau_m^{n,n'}$ is the additional delay difference between echo n and n', i.e.,

$$\begin{aligned}m_{\Delta\tau}(t) &= s_{bb}(t)s_{bb}(t-\Delta\tau)\\ \Delta\tau_m^{n,n'} &= \tau_m^{n'}-\tau_m^n.\end{aligned} \qquad (83)$$

Furthermore, since $b_m(t-t_m^\kappa-\tau_m^0)^2 = b_m(t-t_m^\kappa-\tau_m^0)$, $\theta_m^{\kappa,n}\sim U[0,2\pi)$ and using trigonometry formula for $\cos(a)\cos(b)$,

$$\begin{aligned}E_f^{n,n'} = \frac{A_m^n A_m^{n'}}{2}E\Big[m_{\Delta\tau_m^{n,n'}}(t-t_m^\kappa-\tau_m^n)b_m(t\\ -t_m^\kappa-\tau_m^0)\Big]\cdot\\ \cos\left(2\pi\left(\Delta f_{D,m}^{n,n'}\right)t+\Delta\theta_m^{n,n'}\right),\end{aligned} \qquad (84)$$

where $\Delta f_{D,m}^{n,n'}$ and $\Delta\theta_m^{n,n'}$ are the difference Doppler frequency and phase between echoes n and n' of beacon m, i.e.,

$$\begin{aligned}\Delta f_{D,m}^{n,n'} &= f_{D,m}^{n'}-f_{D,m}^n\\ \Delta\theta_m^{n,n'} &= \theta_m^{\kappa,n'}-\theta_m^{\kappa,n}.\\ &= \left(\theta_{\mathrm{D},m}^{n'}-\theta_{\mathrm{D},m}^n\right)-\left(\delta\theta_{\mathrm{e},m}^n-\delta\theta_{\mathrm{e},m}^{n'}\right).\end{aligned} \qquad (85)$$

Note that $\Delta\theta_m^{n,n'}$ is deterministic. Assume that the number of pulse pairs emitted during $[-T,T]$ is $\mathrm{K}_m(T)$ then, interchanging sums (where now $\kappa\in[\![1,\mathrm{K}_m(t)]\!]$) and integral

$$\begin{aligned}P_{\mathrm{r}}^{\mathrm{f,c}} &= \lim_{T\to\infty}\frac{1}{T}\sum_{\substack{m,\kappa,n,n'\\ n>n'}}\frac{A_m^n A_m^{n'}}{2}\cdot\\ &\int_{-T}^{T} E\left[m_{\Delta\tau_m^{n,n'}}(t-t_m^\kappa-\tau_m^n)b_m(t-t_m^\kappa-\tau_m^0)\right]\cdot\\ &\cos\left(2\pi\left(\Delta f_{D,m}^{n,n'}\right)t+\Delta\theta_m^{n,n'}\right)dt\end{aligned} \qquad (86)$$

Since $t_m^\kappa\sim U[0,T_0]$ and using Fubini's theorem,

$$\begin{aligned}P_{\mathrm{r}}^{\mathrm{f,c}} &= \lim_{T\to\infty}\frac{1}{T}\sum_{\substack{m,\kappa,n,n'\\ n>n'}}\frac{A_m^n A_m^{n'}}{2T_0}\int_0^{T_0} J(t_m^\kappa)dt_m^\kappa\,,\\ J(t_m^\kappa) &= \int_{-T}^{T} a(t)\cos\left(2\pi\left(\Delta f_{D,m}^{n,n'}\right)t+\Delta\theta_m^{n,n'}\right)dt,\\ a(t) &= b_m(t-t_m^\kappa-\tau_m^0)m_{\Delta\tau_m^{n,n'}}(t-t_m^\kappa-\tau_m^n).\end{aligned} \qquad (87)$$

Therefore, there is no term inside the sum which depends on κ since dependency on t_m^κ is removed by the integral. This yields,

$$
\begin{aligned}
P_{\mathrm{r}}^{\mathrm{f,c}} &= \sum_{\substack{m,n,n' \\ n'>n}} \lim_{T\to\infty} \left(P_{\mathrm{r}}^{\mathrm{f,c},1}(T) \cdot P_{\mathrm{r}}^{\mathrm{f,c},2}(T) \right), \\
P_{\mathrm{r}}^{\mathrm{f,c},1}(T) &= \frac{K_m(T)}{2T}, \\
P_{\mathrm{r}}^{\mathrm{f,c},2}(T) &= \frac{A_m^n A_m^{n'}}{T_0} \int_0^{T_0} J(t_m^\kappa)\, dt_m^\kappa.
\end{aligned} \tag{88}
$$

Assuming that both limits of $P_{\mathrm{r}}^{\mathrm{f,c},1}(T)$ and $P_{\mathrm{r}}^{\mathrm{f,c},1}(T)$ are finites (which will be shown later in the derivation), the limit can be linearized into, as explained in Appendix A,

$$
\begin{aligned}
P_{\mathrm{r}}^{\mathrm{f,c}} &= \sum_{\substack{m,n,n' \\ n'>n}} \lim_{T\to\infty} \left(P_{\mathrm{r}}^{\mathrm{f,c},1}(T) \right) \cdot \lim_{T\to\infty} \left(P_{\mathrm{r}}^{\mathrm{f,c},1}(T) \right), \\
&= \sum_{\substack{m,n,n' \\ n'>n}} \mathrm{PRF_m} \cdot \frac{A_m^n A_m^{n'}}{T_0} \int_0^{T_0} \int_{-\infty}^{\infty} a(t) \cdot \\
&\quad \cos\left(2\pi \left(\Delta f_{D,m}^{n,n'} \right) t + \Delta\theta_m^{n,n'} \right) dt dt_m^\kappa
\end{aligned} \tag{89}
$$

Furthermore, using Parseval's identity and the Hermitian property of the Fourier transform (FT) of a real signal,

$$
\begin{aligned}
&\int_{-\infty}^{+\infty} a(t) \cdot \cos(2\pi f_0 t + \theta)\, dt \\
&\qquad = |A(f_0)| \cos\left(\theta - \phi(f_0) \right),
\end{aligned} \tag{90}
$$

Where $A(f)$ is the FT of $a(t)$ and the function ϕ is the argument of $A(f)$. Therefore, using the definition of $a(t)$ (87) and the change of variable $u = t - t_m^\kappa - \tau_m^n$, f_0 from (90) is identified as $\Delta f_{D,m}^{n,n'}$ and θ as $2\pi\Delta f_{D,m}^{n,n'}(t_m^\kappa + \tau_m^n) + \Delta\theta_m^{n,n'}$. This yields

$$
\begin{aligned}
P_{\mathrm{r}}^{\mathrm{f,c}} &= \sum_{\substack{m,n,n' \\ n'>n}} \mathrm{PRF_m} \cdot \frac{A_m^n A_m^{n'}}{T_0} \int_0^{T_0} \left| M_{\Delta\tau_{\mathrm{m}}^{\mathrm{n,n'}}}^{PB} \left(\Delta f_{D,m}^{n,n'} \right) \right| \cdot \\
&\quad \cos\left(\begin{array}{c} 2\pi\Delta f_{D,m}^{n,n'}(t_m^\kappa + \tau_m^n) + \Delta\theta_m^{n,n'} - \\ \phi\left(M_{\Delta\tau_m^{n,n'}}^{\mathrm{PB}} \left(\Delta f_{D,m}^{n,n'} \right) \right) \end{array} \right) dt_m^\kappa,
\end{aligned} \tag{91}
$$

where

$$
\begin{aligned}
M_{\Delta\tau_{\mathrm{m}}^{\mathrm{n,n'}}}^{PB} \left(\Delta f_{D,m}^{n,n'} \right) &= M_{\Delta\tau_{\mathrm{m}}^{\mathrm{n,n'}}} \left(\Delta f_{D,m}^{n,n'} \right) \\
&\quad * \mathrm{FT}\left(b_m(u + \tau_m^n - \tau_m^0) \right)\Big|_{\Delta f_{D,m}^{n,n'}}
\end{aligned} \tag{92}
$$

Finally, $M_{\Delta\tau_{\mathrm{m}}^{\mathrm{n,n'}}}^{PB} \left(\Delta f_{D,m}^{n,n'} \right)$ does not depend on t_m^κ and therefore the integral in (91) has a well-known closed-form from typical GNSS correlator output derivation such that [27]

$$
\begin{aligned}
P_{\mathrm{r}}^{\mathrm{f,c}} &= \sum_{\substack{m,n,n' \\ n'>n}} \mathrm{PRF_m} A_m^n A_m^{n'} \left| M_{\Delta\tau_{\mathrm{m}}^{\mathrm{n,n'}}}^{\mathrm{PB}} \left(\Delta f_{D,m}^{n,n'} \right) \right| \cdot \\
&\quad \mathrm{sinc}\left(\pi\Delta f_{D,m}^{n,n'} T_0 \right) \cos(\pi\Delta f_{D,m}^{n,n'}(T_0 + 2\tau_m^n) + \\
&\quad \Delta\theta_m^{n,n'} - \phi\left(M_{\Delta\tau_m^{n,n'}}^{\mathrm{PB}} \left(\Delta f_{D,m}^{n,n'} \right) \right))
\end{aligned} \tag{93}
$$

which concludes the derivation of $P_{\mathrm{r}}^{\mathrm{f,c}}$.

REFERENCES

[1] RTCA, "DO 292 - Assessment of Radio Frequency Interference Relevant to the GNSS L5/E5A Frequency Band," Jul. 2004.

[2] F. Bastide, "Analysis of the Feasibility and Interests of Galileo E5a/E5b and GPS L5 for Use with Civil Aviation," Institut National Polytechnique de Toulouse, France, 2004.

[3] J. Betz, "Effect of Partial-Band Interference on Receiver Estimation of C/N0: Theory," in *2001 National Technical Meeting of The Institute of Navigation*, Long Beach, California, Jan. 2001.

[4] J. Jang, M. Paonni, and B. Eissfeller, "CW Interference Effects on Tracking Performance of GNSS Receivers," *IEEE Trans. Aerosp. Electron. Syst.*, vol. 48, no. 1, pp. 243–258, Jan. 2012.

[5] A. T. Balaei, A. G. Dempster, and L. L. Presti, "Characterization of the Effects of CW and Pulse CW Interference on the GPS Signal Quality," *IEEE Trans. Aerosp. Electron. Syst.*, vol. 45, no. 4, pp. 1418–1431, Oct. 2009.

[6] C. Hegarty, A. J. Van Dierendonck, D. Bobyn, M. Tran, T. Kim, and J. Grabowski, "Suppression of Pulsed Interference through Blanking," presented at the Proceedings of the Institute of Navigation Annual Meeting, Fairvax, VA, Jun. 2000.

[7] C. Hegarty, T. Kim, S. Ericson, P. Reddan, T. Morrissey, and A. J. Van Dierendonck, "Methodology for Determining Compatibility of GPS L5 with Existing Systems and Preliminary Results," presented at the Proceedings of The Institute of Navigation Annual Meeting, Cambridge, MA, Jun. 1999.

[8] T. Kim and J. Grabowski, "Validation of GPS L5 Coexistence with DME/TACAN and Link-16 Systems," in *16th International Technical Meeting of The Satellite Division of the Institute of Navigation*, Portland, Oregon, Sep. 2003.

[9] F. Bastide, E. Chatre, C. Macabiau, and B. Roturier, "GPS L5 and GALILEO E5a/E5b signal-to-noise density ratio

degradation due to DME/TACAN signals : simulations and theoretical derivation," presented at the Proceedings of the 2004 National Technical Meeting of the Institue of Navigation, 2004, pp. 1049–1062.
[10] A. Garcia-Pena, C. Macabiau, M. Mabilleau, and P. Durel, "Impact of DME/TACAN on GNSS L5/E5a Receiver," presented at the ITM 2020, International Technical Meeting, San Diego, California, Jan. 2020.
[11] A. Garcia-Pena, C. Macabiau, J. Ashley, D. Baraban, P. Durel, and M. Mabilleau, "Model and observation of the impact of JTIDS/MIDS on GNSS C/N0 degradation," presented at the PLANS 2020 IEEE/ION Position, Location and Navigation Symposium, Portland, Oregon, Apr. 2020.
[12] A. Garcia-Pena, O. Julien, P. V. Gakne, C. Macabiau, M. Mabilleau, and P. Durel, "Efficient DME/TACAN Blanking Method for GNSS-based Navigation in Civil Aviation," presented at the ION GNSS+ 2019, 32nd International Technical Meeting of the Satellite Division of The Institute of Navigation, Miami, Florida, Sep. 2019.
[13] A. Garcia-Pena, O. Julien, C. Macabiau, M. Mabilleau, and P. Durel, "GNSS C/N0 degradation model in presence of continuous wave and pulsed interference," NAVIGATION.2021;68:75–91.
[14] Zeta associates, "High L5 Blanking at HNL WRS HNL TACAN Study" *RTCA SC-159 WG-6 presentation*, Mar. 2019, *internal.*
[15] Zeta associates, "High L5 Blanking at ZLA WRS, update to HNL TACAN Study" *RTCA SC-159 WG-6 presentation*, Oct. 2021, *internal.*
[16] N. Gault, A. Chabory, A. Garcia-Pena, and C. Macabiau, "DME/TACAN multipath Impact on GNSS L5/E5a Airborne Receivers Part II: Air-To-Ground Channel Model and Application," *IEEE Trans. Aerosp. Electron. Syst.*, submitted.
[17] W. Burnside and K. Burgener, "High frequency scattering by a thin lossless dielectric slab," *IEEE Trans. Antennas Propag.*, vol. AP-31, no. 1, pp. 104–110, Jan. 1983.
[18] N. Gault, A. Garcia-Pena, A. Chabory, and C. Macabiau, "Impact of DME/TACAN on GNSS L5/E5a Receiver at Low Altitude Considering Multipath," presented at the Proceedings of the 35th International Technical Meeting of the Satellite Division of the Institute of Navigation (ION GNSS+ 2022), Denver, Sep. 2022.
[19] R. C. Borden, C. C. Trout, and E. C. Williams, "Description and evaluation of 100-channel Distance-Measuring Equipment," presented at the Proceedings of the IRE, vol. 39, no. 6, pp. 612-618, doi: 10.1109/JRPROC.1951.233461., Jun. 1951.
[20] M. Kayton and W. R. Freid, *Avionics Navigation Systems*, Second Edition. in Wiley, pp.133-138. New York, 1969.
[21] F. Bastide, D. Akos, C. Macabiau, and B. Roturier, "Automatic Gain Control (AGC) as an Interference Assessment Tool," in *16th International Technical Meeting of The Satellite Division of the Institute of Navigation*, Portland, Oregon, Sep. 2003. Accessed: May 27, 2016.
[22] International Civil Aviation Organization (ICAO), *International standards and recommended practices for aeronautical telecommunications*, Annex 10 to the convention of international civil aviation. 2020.
[23] J. W. Betz and K. Kolodziejski, "Generalized Theory of Code Tracking with an Early-Late Discriminator Part I: Lower Bound and Coherent Processing," *IEEE Trans. Aerosp. Electron. Syst.*, vol. 45, no. 4, pp. 1538–1556, Oct. 2009.
[24] L. Kleinrock, *Queing Systems*, vol. 1. New York: John Wiley & Sons, 1975.
[25] F. Bastide, "Galileo E5a/E5b and GPS L5 Acquisition Time Statistical Characterization and Application to Civil Aviation," in *Proc. 2004 Nat. Tech. Meeting Inst. Navigation*, Long Beach, California, Sep. 2004, pp. 1049–1062.
[26] Skybrary, "Approach Speed Categorisation." 2023.
[27] B. Parkinson and J. Spiker, *Progress in astronautics and aeronautics: Global positioning system: Theory and applications,* vol. 1. 1996.

Nicolas Gault graduated as an electronic engineer from ENAC (École Nationale de l'Aviation Civile) Toulouse, France, in 2020. He is now a Ph.D student at the TELECOM lab of ENAC. His Ph.D topic deals with the model of impact of interferences on the GNSS L5/E5a band. He recently spent 6 months at the RF & SatNav laboratory of the University of Colorado, Boulder, for collaborative research.

Axel Garcia-Pena is a researcher/lecturer with the SIGnal processing and NAVigation (SIGNAV) research axis of the TELECOM lab of ENAC (French Civil Aviation University), Toulouse, France. His research interests are GNSS navigation message demodulation, optimization and design, GNSS receiver design and GNSS satellite payload. He received his double engineer degree in 2006 in digital communications from SUPAERO and UPC, and his PhD in 2010 from the Department of Mathematics, Computer Science and Telecommunications of the INPT (Polytechnic National Institute of Toulouse), France.

Alexandre Chabory received the M.Sc. degree in electrical engineering from ENAC, the French Civil Aviation University, Toulouse, in 2001, and the Ph.D. degree from Paul Sabatier University, Toulouse, in 2004. From 2004 to 2007, he was a Post-Doctoral Scientist with the Eindhoven University of Technology, the Netherlands. Since 2007, he has been with ENAC where he is now full-professor and head of the electromagnetics and antennas research group. His research interests include electromagnetic theory and modeling, mainly for aeronautical applications.

Christophe Macabiau graduated as an electronic engineer in 1992 from the ENAC (Ecole Nationale de l'Aviation Civile) in

Toulouse, France. Since 1994, he has been working on the application of satellite navigation techniques to civil aviation. He received his Ph.D in 1997 and has been in charge of the signal processing lab of ENAC since 2000, where he also started dealing with navigation techniques for terrestrial navigation. He is currently the head of the TELECOM team of ENAC, that includes research groups on signal processing and navigation, electromagnetics, and data communication networks.

Loïc Shi-Garrier is a PhD student at Ecole Nationale de l'Aviation Civile. He received a master's degree in aerospace engineering in 2020 and a master's degree in operational research in 2021, both from ENAC. He is interested in robust machine learning, differential geometry, and air traffic flow and capacity management.